RI 9529

REPORT OF INVESTIGATIONS/1995



# Active Control of Underground Stresses Through Rock Pressurization

By Thomas L. Vandergrift

UNITED STATES DEPARTMENT OF THE INTERIOR

BUREAU OF MINES

## *U.S. Department of the Interior*
## *Mission Statement*

As the Nation's principal conservation agency, the Department of the Interior has responsibility for most of our nationally-owned public lands and natural resources. This includes fostering sound use of our land and water resources; protecting our fish, wildlife, and biological diversity; preserving the environmental and cultural values of our national parks and historical places; and providing for the enjoyment of life through outdoor recreation. The Department assesses our energy and mineral resources and works to ensure that their development is in the best interests of all our people by encouraging stewardship and citizen participation in their care. The Department also has a major responsibility for American Indian reservation communities and for people who live in island territories under U.S. administration.

Report of Investigations 9529

# Active Control of Underground Stresses Through Rock Pressurization

By Thomas L. Vandergrift

UNITED STATES DEPARTMENT OF THE INTERIOR
Bruce Babbitt, Secretary

BUREAU OF MINES
Rhea L. Graham, Director

International Standard Serial Number
ISSN 1066-5552

# CONTENTS



## ILLUSTRATIONS

## ILLUSTRATIONS—Continued



## TABLES



## UNIT OF MEASURE ABBREVIATIONS USED IN THIS REPORT

Metric Units

| | | | |
|---|---|---|---|
| cm | centimeter | N | newton |
| m | meter | N•m | newton meter |
| MPa | megapascal | °C | degree Celsius |
| mPa•s | millipascal second | | |

U. S. Customary Units

| | | | |
|---|---|---|---|
| cP | centipoise | lbf | pound force |
| ft | foot | P | poise |
| ft•lb | foot pound (force) | psi | pound per square inch |
| in | inch | °F | degree Fahrenheit |

# ACTIVE CONTROL OF UNDERGROUND STRESSES THROUGH ROCK PRESSURIZATION

By Thomas L. Vandergrift[1]

## ABSTRACT

To significantly increase the stability of underground excavations while exploiting the full advantages of confined rock strength, methods must be developed to actively control the distribution of stresses near the excavation. This U.S. Bureau of Mines study examines theoretical and practical aspects of rock pressurization, an active stress control concept that induces compressive stress in the wall rock through repeated hydraulic fracturing with a settable fluid.

Numerical analyses performed by incorporating the rock pressurization concept into a variety of boundary-element models indicate that rock pressurization has the potential to improve underground excavation stability in three ways: (1) by relocating stress concentrations away from the weak opening surface to stronger, confined wall rock; (2) by inducing additional stresses in a biaxial stress field to reduce the difference between the principal stress components near the surface of the opening; and (3) by counteracting the tensile stresses induced in the rock around internally loaded openings.

Practical aspects of the rock pressurization concept were investigated through a series of hydraulic fracturing experiments. The use of sulfur as a settable fluid for hydraulic fracturing was demonstrated, although problems related to sulfur viscosity suggest that other molten materials, such as wax, may be better suited to practical field application of the rock pressurization concept.

[1]Mining engineer, Denver Research Center, U.S. Bureau of Mines, Denver, CO.

## INTRODUCTION

When an underground opening is made, loads originally supported by the excavated material are redistributed around the opening. This stress redistribution is usually allowed to occur naturally; stresses are then concentrated on the intact opening surface where the rock is unconfined and relatively weak. This combination of high stress and low strength can lead to several types of opening instability, ranging from minor cracking and spalling to violent failures such as rock bursts, floor heaves, and roof falls. Stress-related stability problems become more acute as deeper openings are excavated, as the areas of influence of different openings interact, and when high tectonic stresses are encountered. A largely unexplored and unexploited method of increasing the stability of underground openings involves the development of active stress control measures to govern both the magnitude and location of stress concentrations around the excavation.

Several investigators have recognized that excavation stability can be improved by inducing compressive stresses near the opening. It has been proposed that induced compressive stresses can improve excavation stability in two different ways: by compressing strata prone to tensile failure (*1-2*),[2] or through the formation of a pressure arch within the wall rock to reduce tangential stress concentrations on the opening surface (*3*). Methods for inducing compression in the wall rock surrounding an excavation have been suggested; however, none have been developed sufficiently for practical field application.

This report documents the results of a U.S. Bureau of Mines investigation into rock pressurization, a potentially practical means of inducing compressive stresses for active stress control and improved opening stability. Theoretical aspects of the concept were studied using numerical modeling techniques. Boundary-element models incorporating the rock pressurization concept applied to a variety of underground excavation situations were run to study the effects of induced compressive stress on opening stability. Practical aspects of rock pressurization were studied through a series of laboratory experiments. Attempts were made to internally induce compressive stresses in a confined concrete block by repeated hydraulic fracturing. As a prelude to this effort, unconfined concrete cubes were hydraulically fractured with sulfur to evaluate sulfur as an injection fluid and to study injection system variables.

## CONCEPT OF ACTIVE STRESS CONTROL

Active stress control is a concept not currently used in the design of underground structures. It refers to the ability to manipulate both the magnitude and location of stress concentrations in the rock surrounding an excavation. As such, active stress control is a departure from traditional stress management techniques.

In the past, variations in excavation geometry and rock support capacity have been used to mitigate stress-related ground control problems. Geometric factors that can be varied include excavation location, shape, and orientation with respect to the in situ stress field (*4*); excavation sequence (*5*); and the configuration of multiple openings (*6*). Often, however, operational constraints dictate excavation geometry. In other cases, stress conditions are so adverse that geometry-based solutions are not adequate. When geometric solutions are impractical or inadequate, destressing techniques have been used. Destressing reduces stress concentrations by lowering the support capacity of the treated rock. Destressing was first introduced in South Africa in the mid-1950's (*7*). Since then, several variations have been developed, including undersizing pillars so that they yield in a controlled manner (*8-9*), drilling to reduce pillar strength (*10-11*), blasting to initiate stress relief (*12-13*), and injecting water to reduce the normal stress across weakness planes (*14*).

Although geometric and destressing methods can be effective in certain situations, both are passive forms of stress control; they cannot simultaneously control the magnitude and location of stress concentrations around the underground excavation. Optimizing opening geometry can reduce the magnitude of tangential stress concentrations on the opening surface, but cannot shift those high stress concentrations from the unconfined opening surface to the confined wall rock. Destressing offers a kind of "negative" stress control; stress concentrations are shifted from the treated area but the destination of the redistributed stress is not controlled. Also, by its nature, destressing reduces the integrity of the structure.

In order to develop more active forms of stress control, the challenges and opportunities that are unique to the underground environment must be clearly understood. In

[2]Italicized numbers in parentheses refer to items in the list of references preceding the appendixes.

surface structures, stresses can be managed by choosing structural materials with acceptable strength and deformational characteristics. Structural material choices are limited for underground structures, which consist almost exclusively of the rock that the excavation is driven through. However, the underground environment provides an important benefit that is available nowhere else—confinement.

Since the work of Coulomb in 1773, it has been recognized that rock strength is increased by confinement. Examples of this increase in ultimate compressive strength are shown in figure 1 for different rock types loaded triaxially. In a triaxial test, rock is confined by hydraulic pressure. Underground, the rock is self-confined: its degree of confinement depends on its boundary conditions, especially the distance to free surfaces such as openings. So while the nature of underground construction limits structural material choices, rock confinement, and therefore rock strength, changes within the structure. The challenge is to control the distribution of stresses within the wall rock to take advantage of this inherent "strength of position" (*16*). Without more active forms of stress control, in which both the magnitude and location of stresses are controlled, the full advantages of confined rock strength will never be realized.

## PRIOR RESEARCH

The concept of inducing compressive stresses for active stress control may have originated with Reed in the 1950's

***Figure 1***

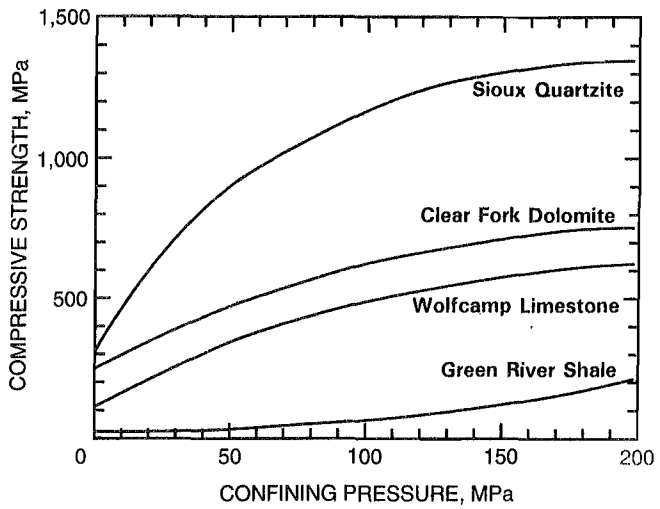


***Increase in rock compressive strength as a function of confining pressure (15).***

(*3*). Using pressure tubes embedded in plaster models, he demonstrated that stresses on the surface of the model opening could be reduced by forming a tangential compression arch in the model wall. By pressurizing the tubes to between two and four times the external hydrostatic loading, he was able to reduce tangential stress concentrations on the opening surface by up to 20%. He suggested that similar results could be obtained in the field by inserting wedges in radially oriented boreholes to induce compressive stress tangent to the opening surface. This suggestion is not practical, since the wedge-induced stresses would diminish within about four borehole radii. In order for the effects of the wedges to overlap, an excessive number of closely spaced boreholes would have to be drilled.

A similar borehole approach was patented by Whiting (*2*). He proposed using "rock jacks" to hold rock blocks together in the roof or back, thereby decreasing the likelihood of gravity falls. His rock jack is essentially a hollow roof bolt that can be inserted in a borehole and internally pressurized with hydraulic fluid. While such a device could be used to induce compressive stresses in a localized area, it is impractical for active stress control for the same reasons cited above.

A method of inducing compressive stresses whose influence is not tied to the borehole radius has been proposed by Colgate (*17*). Colgate's method involves the hydraulic fracturing of rock with a settable fluid. Conceptually, the fluid is injected into a packed-off borehole (figure 2*A*). Continued injection increases the fluid pressure and changes the stress distribution in the borehole wall. When the tangential tensile stress at the surface of the borehole wall overcomes the tensile strength of the rock, fracturing occurs and a fracture plane extends perpendicular to the minimum (least compressive) principal stress direction (figure 2*B*). Injection is then stopped, and the fluid is allowed to set in the fracture. As the fluid sets, compressive stresses induced normal to the plane of the fracture are maintained. Repeated fracturing increases the local minimum principal stress until it becomes greater than the original intermediate principal stress. Subsequent fractures form perpendicular to this new local minimum principal stress direction (figure 2*C*). Additional fracturing cycles further reorient the induced fracture direction, and eventually a roughly spherical volume of pressurized rock hundreds of times the radius of the borehole is formed (figure 2*D*).

Colgate and his coworkers have addressed some of the theoretical questions related to this "pressure sphere" concept and have proposed its use in a variety of underground excavation applications. These applications include the compression of rock prone to tensile failure (*1, 17-20*), the

*Figure 2*

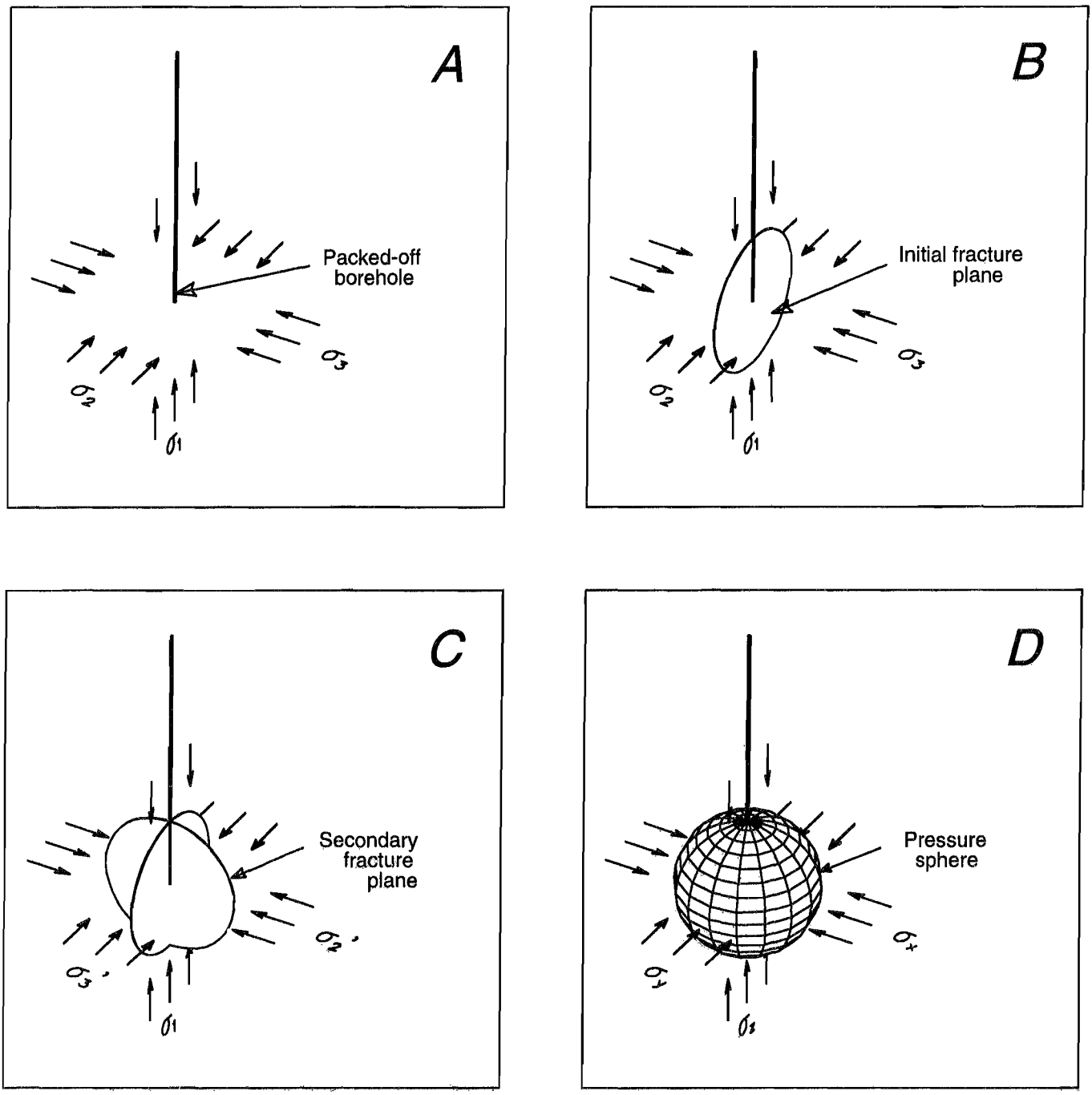


***Conceptual creation process for pressure spheres. A, Fluid injection into a packed-off borehole; B, initial fracture plane perpendicular to the minimum ($\sigma_3$) principal stress direction, in the plane of the maximum ($\sigma_1$) and intermediate ($\sigma_2$) principal stresses; C, secondary fracture plane perpendicular to the rotated local minimum principal stress ($\sigma_3$') direction; D, roughly spherical pressurized region, with local principal stresses $\sigma_x = \sigma_y = \sigma_z$.***

creation of underground voids by lifting overburden (*1*, *17-18*), the formation of barriers to gas flow (*1*, *21*), and the design of nuclear waste repositories (*20*).

The pressure sphere method has been attempted in the field on two occasions (*18*, *22*). Based on measured increases in the fracture extension pressure for successive fracturing cycles, Colgate surmised that zones of pressurized rock were formed. However, the overall success of these attempts is hard to judge due to a lack of quantitative data.

Although active stress control concepts are not new, their potential for controlling the stress distribution around underground excavations has not been fully explored. Theoretical research has shown that properly oriented, induced compressive stresses can be beneficial to opening stability. However, practical methods of inducing oriented stresses have not been developed. The pressure sphere method appears to have the potential for practical application, but is nondirectional. In order to achieve the improvements in opening stability shown to be theoretically possible, practical rock pressurization methods, with controlled induced-stress orientation, must be developed.

*Figure 3*

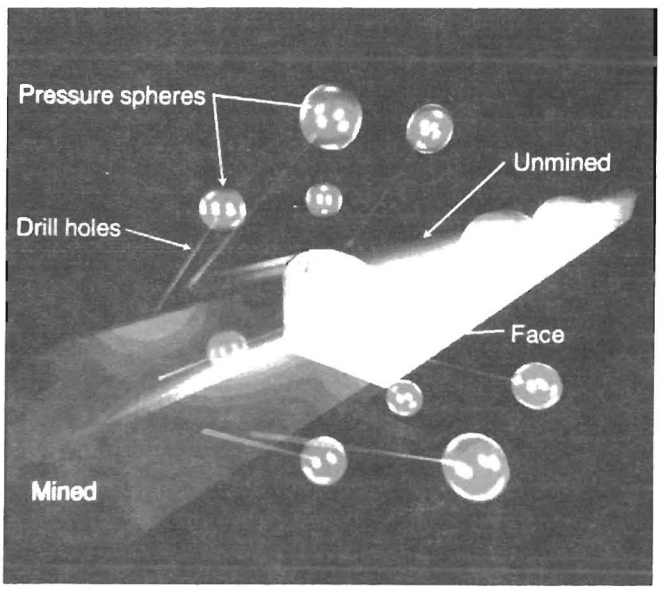


*Pressure sphere formation prior to heading advance.*

## CONCEPTUAL PRESSURIZATION PROCESS

The rock pressurization concept is based on the assumption that zones of enhanced compressive stress can be formed in a controlled manner and arranged in such a way that they will have a beneficial effect on the stress distribution near an excavation. Assuming that individual "spheres" of pressurized rock can be created as described by Colgate, and that the pressure spheres can be maintained over the useful life of the excavation, it is envisioned that the process of rock pressurization would be applied in the following manner. A ring of pressure spheres would be formed prior to heading advance from boreholes angled ahead of the face (figure 3). Sphere location would be dictated by the length and inclination of the boreholes. Individual boreholes would then be packed off, and the process of repeated hydraulic fracturing begun. Sphere pressure and extent would be controlled by monitoring injection volumes and pressures. In this manner, a specified stress distribution would be defined ahead of the face prior to heading advance (figure 4).

*Figure 4*

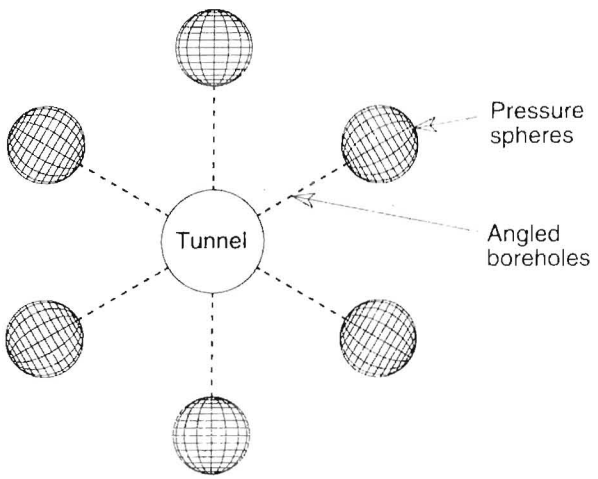


*Pressure spheres arranged around an opening to produce a prescribed stress distribution, as indicated by principal stress trajectories.*

## NUMERICAL MODELING ANALYSIS

An evaluation of rock pressurization and its potential for improving opening stability was performed using numerical modeling methods. Two-dimensional, boundary-element models incorporating the pressure sphere concept were analyzed for a variety of excavation scenarios. The goals of this analysis were to—

- Study the underlying mechanisms associated with rock pressurization and to explain how it can be applied to improve opening stability;
- Evaluate the effects of sphere parameters such as arrangement, size, and pressure on the induced stress distribution around circular underground openings; and
- Demonstrate specific applications for the rock pressurization concept.

The key to the numerical analysis of rock pressurization lies in the representation of the pressure spheres. Because only limited work has been done to physically demonstrate the pressure sphere concept, gross assumptions were required with regard to sphere parameters, including the mechanisms of sphere formation, sphere dimensions, and the pressures developed within the spheres. The laboratory portion of this research was designed, in part, to test the soundness of these assumptions. As with any modeling analysis, the overall validity depends on how well the models represent actual physical phenomena.

Prior to performing the numerical analysis, a simplified method of modeling the pressure sphere concept was developed. It was decided to represent, in two dimensions, the spheres by circular holes oriented parallel to the long axis of the modeled opening. Hydrostatic load applied within these holes or "pressure cylinders" were used to model pressure spheres formed by sequential, reoriented hydraulic fracturing. Details of pressure sphere model development, and of the boundary-element program used in the analysis, are given in appendix A.

### GENERAL EFFECTS OF PRESSURIZATION ON THE UNDERGROUND STRESS DISTRIBUTION

Using internally loaded, circular openings to represent pressure spheres, several models were run to determine the effects of sphere pressure, placement, and diameter on the underground stress distribution. To compare one model with another, distributions of maximum (most compressive) principal stress, minimum (least compressive) principal stress, relative displacement, and strength factor were examined. Using the Mohr-Coulomb failure criterion, strength factor is defined as the ratio of the maximum internal shear stress at failure for a given point to the maximum internal shear stress developed at that point. Strength factors less than one indicate instability (see appendix A for details of the strength factor calculation). As with all models discussed in this report, compressive stresses were taken to be positive. Because of symmetry, only one quadrant of each model is shown.

To establish a baseline, the simple case of a circular opening in a hydrostatic stress field of 69 MPa (10,000 psi) was modeled. The maximum principal stress contours around the opening are shown in figure 5*A*.[3] In agreement with the analytic solution, the boundary-element results show that the tangential stress concentration on the opening surface is two, and falls off to the field stress within about four opening radii. The minor principal stresses (figure 5*B*), which are oriented radially, are zero at the opening surface and gradually approach the field stress, again within about four opening radii. Using physical properties assumed for granite (see appendix A), the calculated strength factor on the opening surface is 1.0 (figure 5*C*), which indicates that the opening is very close to failure. The induced displacement vectors (figure 5*D*) point toward the center of the opening.

To study the effects of pressurized spheres on the stress distribution near the opening, six pressure spheres were placed around the opening at 60° intervals. Figure 6*A* shows the maximum principal stress contours that result from a ring of 4.6-m-diam (15-ft-diam) spheres with internal pressures of 310 MPa (45,000 psi). The spheres are centered 11.4 m (37.5 ft) from the model origin (which coincides with the center of the opening). The spheres result in increased tangential stresses on the opening surface. Before introducing the pressure spheres, the tangential stress on the opening surface was 138 MPa (20,000 psi). With the spheres, tangential surface stresses are in the 138- to 152-MPa (20,000- to 22,000-psi) range. The minimum principal stress distribution (figure 6*B*) shows that tensile stresses surrounding the pressure spheres do not extend to the opening; therefore, pressurization does not contribute to tensile failure near the opening. Strength factors near the opening fall below one (figure 6*C*), indicating that this arrangement of pressure spheres is detrimental to opening stability.

The stresses and displacements calculated in this analysis arise from a linear combination of the effects of the field stresses, the opening, and the pressure spheres. To isolate the effects of the pressure spheres alone, models with no opening or field stress were run. Figure 7 shows

[3]Because the original work was performed in U.S. customary units, contours on this and subsequent plots are in intervals of psi. To convert from psi to MPa, divide by 145.

*Figure 5*

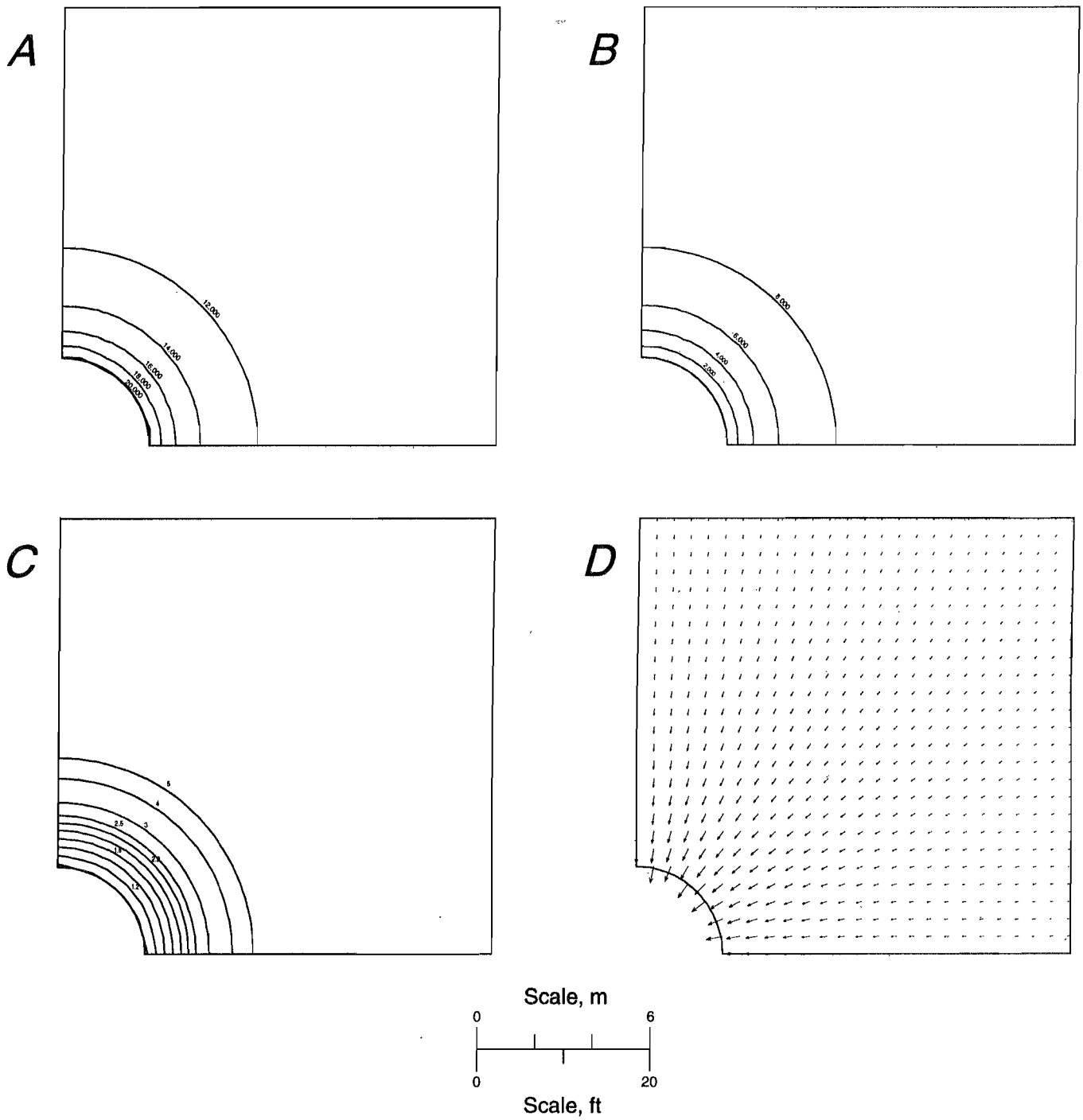


***Circular opening in a 69 MPa 10,000 psi hydrostatic stress field. A, Maximum principal stress distribution; B, minimum principal stress distribution; C, strength factor distribution; D, relative displacement.***

*Figure 6*

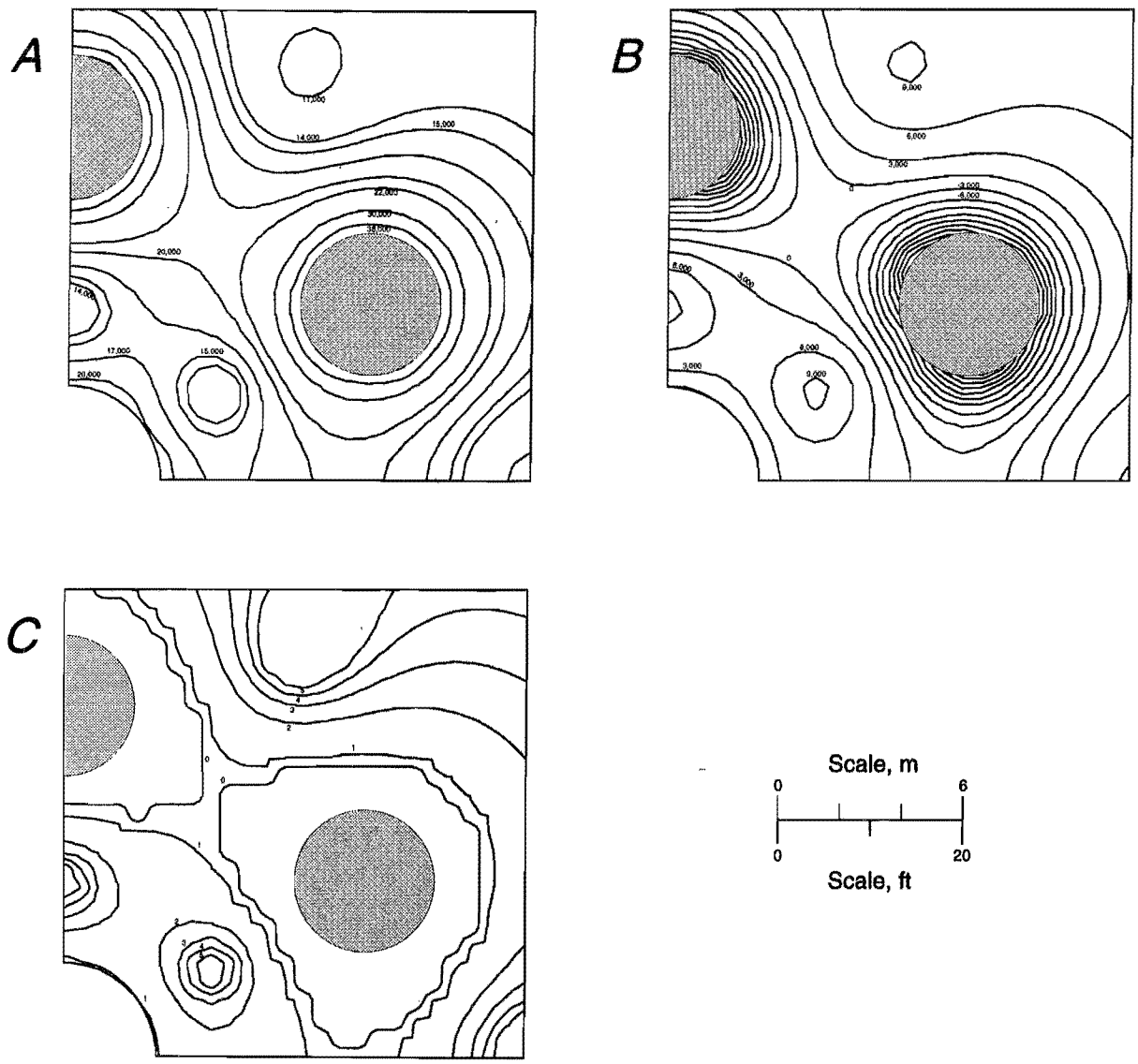


*Single ring of 310-MPa (45,000-psi) pressure spheres 11.4 m (37.5 ft) arranged around a circular opening in a hydrostatic stress field. A, Maximum principal stress distribution; B, minimum principal stress distribution; C, strength factor distribution.*

the maximum principal stress distribution induced by the 310-MPa (45,000-psi) pressure spheres. In the area where the opening would be located, compressive stresses approaching 13.8 MPa (2,000 psi) are induced.

Because the induced stresses and displacements are proportional to the applied stresses, changing the sphere pressure simply changes the magnitude of induced stress. Figure 8*A* shows the maximum principal stress distribution induced by a ring of 207-MPa (30,000-psi) pressure spheres. In comparing this model with the base model, the 13.8-MPa (2,000-psi) contour is farther from the model origin. When sphere pressure is increased to 414 MPa (60,000 psi) (figure 8*B*), stresses induced near the potential opening boundary are increased to between 13.8 and 27.6 MPa (2,000 and 4,000 psi).

The effects of sphere location were studied by varying the distance of the spheres from the model center. Maximum principal stress contours for 310-MPa (45,000-psi), 4.6-m-diam (15-ft-diam) spheres located 9 m (30 ft) from the model origin are shown in figure 9*A*. Moving the spheres in toward the model center increases induced stresses in the area where the opening would be located,

***Figure 7***

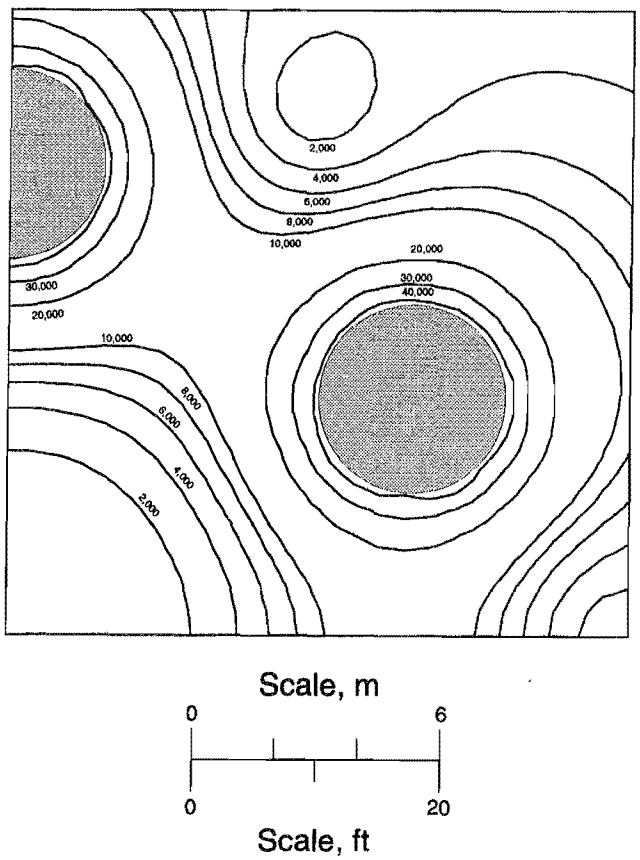


***Single ring of 310-MPa (45,000-psi) pressure spheres in a model with no opening or field stress, maximum principal stress distribution.***

***Figure 8***

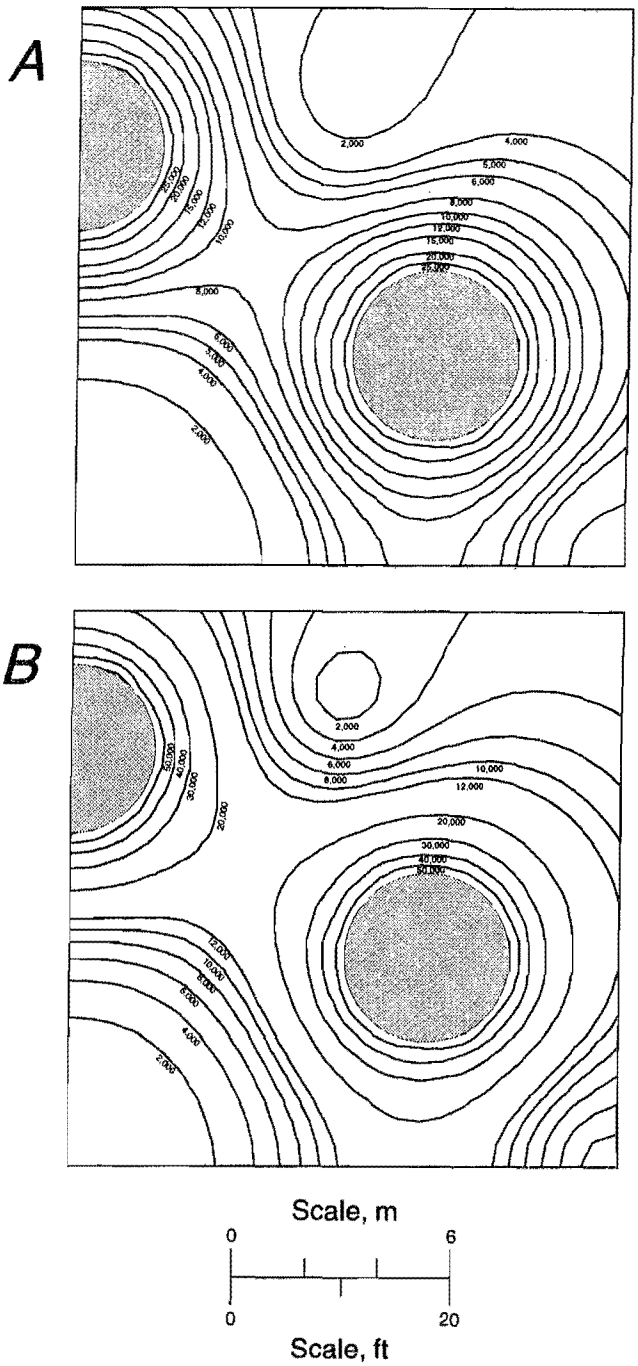


***Single ring of: A, 207-MPa (30,000-psi) and B, 414-MPa (60,000-psi) pressure spheres; in a model with no opening or field stress, maximum principal stress distribution.***

in this case to between 13.8 and 27.6 MPa (2,000 and 4,000 psi). Moving the spheres out to 13.7 m (45 ft) from the center reduces the induced stresses in this area below 13.8 MPa (2,000 psi) (figure 9*B*).

***Figure 9***

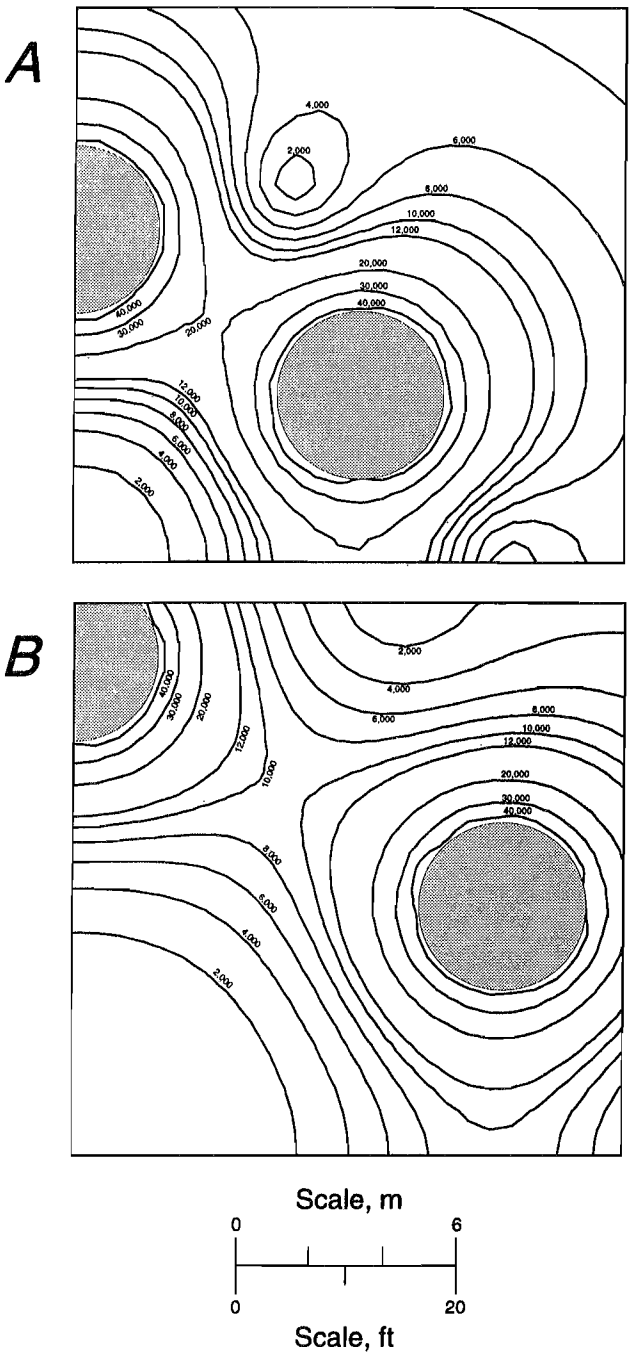


*Single ring of 310-MPa (45,000-psi) pressure spheres. A, 9.1 m (30 ft); and B, 13.7 m (45 ft); from the center of a model with no opening or field stress, maximum principal stress distribution.*

The 4.6-m (15-ft) sphere diameter in the previous models was arbitrarily chosen. Figure 10 shows that reducing sphere diameter to 3 m (10 ft), while keeping sphere pressure at 310 MPa (45,000 psi) and the distance from the model center at 11.4 m (37.5 ft), reduces stresses near the model center. The effects of reduced sphere diameter are similar to the effects of reduced sphere pressure (figure 8*A*).

With an understanding of the general effects of pressure spheres on the stress distribution near an underground opening, specific applications for the pressurization concept were investigated.

## PRESSURIZATION APPLIED TO REDUCE COMPRESSIVE STRESS CONCENTRATIONS ON THE OPENING SURFACE

As noted earlier, the shortcoming of Reed's suggestion for active stress control is that practical methods of inducing the required tangential stresses have not been

***Figure 10***

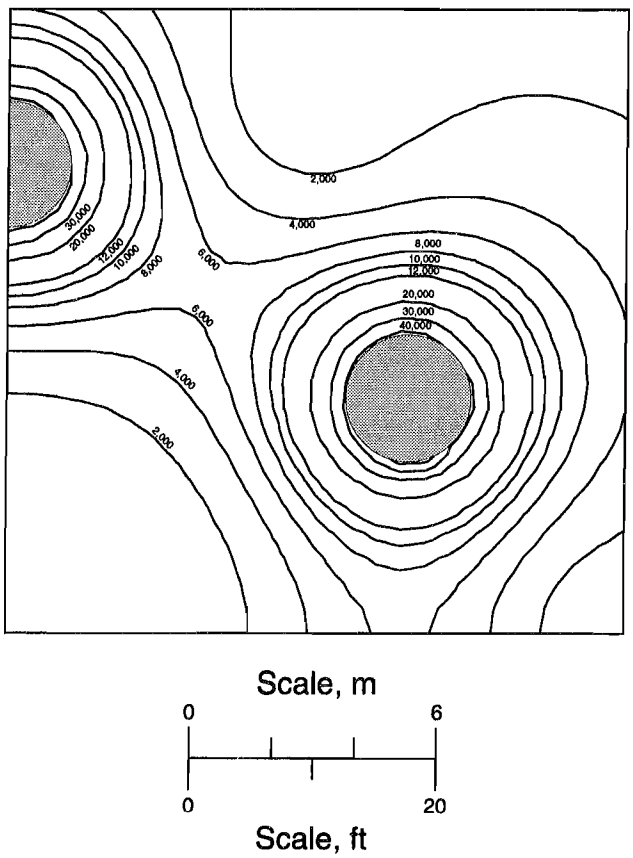


*Single ring of 3-m (10-ft) diam, 310-MPa (45,000-psi) pressure spheres 11.4 m (37.5 ft) arranged around the center of a model with no opening or field stress.*

developed. In an attempt to demonstrate that tangential stress concentrations on the opening surface can be relocated to stronger, confined wall rock using practical methods, a series of models was run with a variety of pressure sphere arrangements surrounding the opening.

Oudenhoven (*16*) extended the work of Reed by performing a finite-element analysis of pressurized slots in the vicinity of an opening. This analysis is duplicated here using the boundary-element method. The pressurized slot model consists of four 6.1-m-long (20-ft-long) by 0.3-m-wide (1-ft-wide) slots located at 90° intervals around a 6.1-m-diam (20-ft-diam) opening. The radially oriented slots have a uniformly distributed stress of 345 MPa (50,000 psi) along their length. The resulting maximum and minimum principal stress distributions are shown in figures 11*A* and 11*B*, respectively. The tangential compressive stresses on the opening surface are reduced to less than 41 MPa (6,000 psi), with small zones of tangential tensile stress in the back and rib. This is a significant reduction from the uniform, compressive tangential stress of 138 MPa (20,000 psi) that exists on the surface without the slots (figure 5*A*). The calculated strength factors on the opening surface with the slots are in the 1.5 to 3.5 range (figure 11*C*), indicating an increase in opening stability of at least 50%. By removing the opening and field stress, the effects of the slots can more readily be seen. Figure 12*A* shows that the pressurized slots produce a region of tensile stress where the opening would be located. The induced tensile stress lessens the magnitude of compressive stress concentrations that result from the field stresses and the presence of the opening. At the same time, a ring of compressive stress is induced around the model center. The displacements associated with the induced stresses are shown in figure 12*B*. The loads induced by the slots cause points between the slots to move away from the model origin, in effect "pulling apart" the rock near the center of the model.

In comparing the pressurized slot model with the pressure sphere models previously discussed, it is obvious that the direction of the induced stress is very important in producing the mechanisms necessary for improved opening stability. The pressurized slots produce tangential compressive stresses, while the pressure spheres induce both tangential and radial (with reference to the model origin) compressive stresses. The radial compressive stresses induced by the spheres load the rock in the center of the model, negating the effects of the tangential pressure arch. In order for the pressure spheres to create the mechanisms required to reduce tangential stress concentrations on the opening surface, the induced compressive stresses should be primarily tangential.

In order to induce tangential compressive stresses using Colgate's nondirectional pressure sphere concept, a dual ring of pressure spheres could be used. It is envisioned that a ring of low-pressure spheres could be created around the opening followed by a ring of higher pressure spheres farther into the wall rock. The maximum principal stress distribution for such an arrangement is presented in figure 13*A*. The smaller, inner spheres, centered 7.6 m (25 ft) from the origin, are 3 m (10 ft) in diameter and are pressurized to 103 MPa (15,000 psi). The outer spheres are 4.6 m (15 ft) in diameter, pressurized to 310 MPa (45,000 psi), and located 11.4 m (37.5 ft) from the center. Tangential stresses on the opening surface are reduced from 138 MPa (20,000 psi) (figure 5*A*) to between 48 and 76 MPa (7,000 and 11,000 psi). This reduction is similar to that achieved in the pressurized slot model of Oudenhoven. The minimum principal stress distribution (figure 13*B*) is also similar in that tensile stresses do not extend to the opening. Strength factors near the opening (figure 13*C*) are between 1.2 and 1.6, indicating that significant improvements in opening stability can be achieved using this pressurization arrangement.

A comparison of the radial and tangential stress distribution around the opening with and without the concept of dual sphere pressurization is shown in figure 14. With dual sphere pressurization, tangential stresses on the opening surface are about 0.9 times the field stress, or just 45% of what they would be without pressurization. Tangential stresses are further reduced for a distance into the wall rock of about one-half the opening radius, at which point they increase dramatically to about 3.6 times the field stress at two opening radii. From there, the tangential stresses drop off and approach the field stress. The radial stresses with pressurization are zero at the opening surface, become tensile at about one radius, reach a minimum at about two radii, and then approach the field stress. This figure shows graphically that pressurization reduces stress concentrations on the opening surface and relocates them to stronger, confined wall rock.

The concept of dual sphere pressurization discussed above theoretically would result in improved opening stability. Because of the many unknowns relating to the physical creation of the pressure spheres in this arrangement, attempts to optimize opening stability by modeling various combinations of sphere pressures, locations, and diameters probably would not be meaningful. However, to gain insights into the mechanisms that produce desirable effects on opening stability, a series of models with varying outer sphere pressures was run. In these models, the inner sphere pressure was fixed at 10.3 MPa (1,500 psi) whereas the outer sphere pressure was varied from 34 to 103 MPa (5,000 to 15,000 psi) (see appendix A, figure A-6). By increasing the ratio of outer to inner sphere pressure, the magnitudes of the tensile stresses induced near the model origin are increased. From this it

*Figure 11*

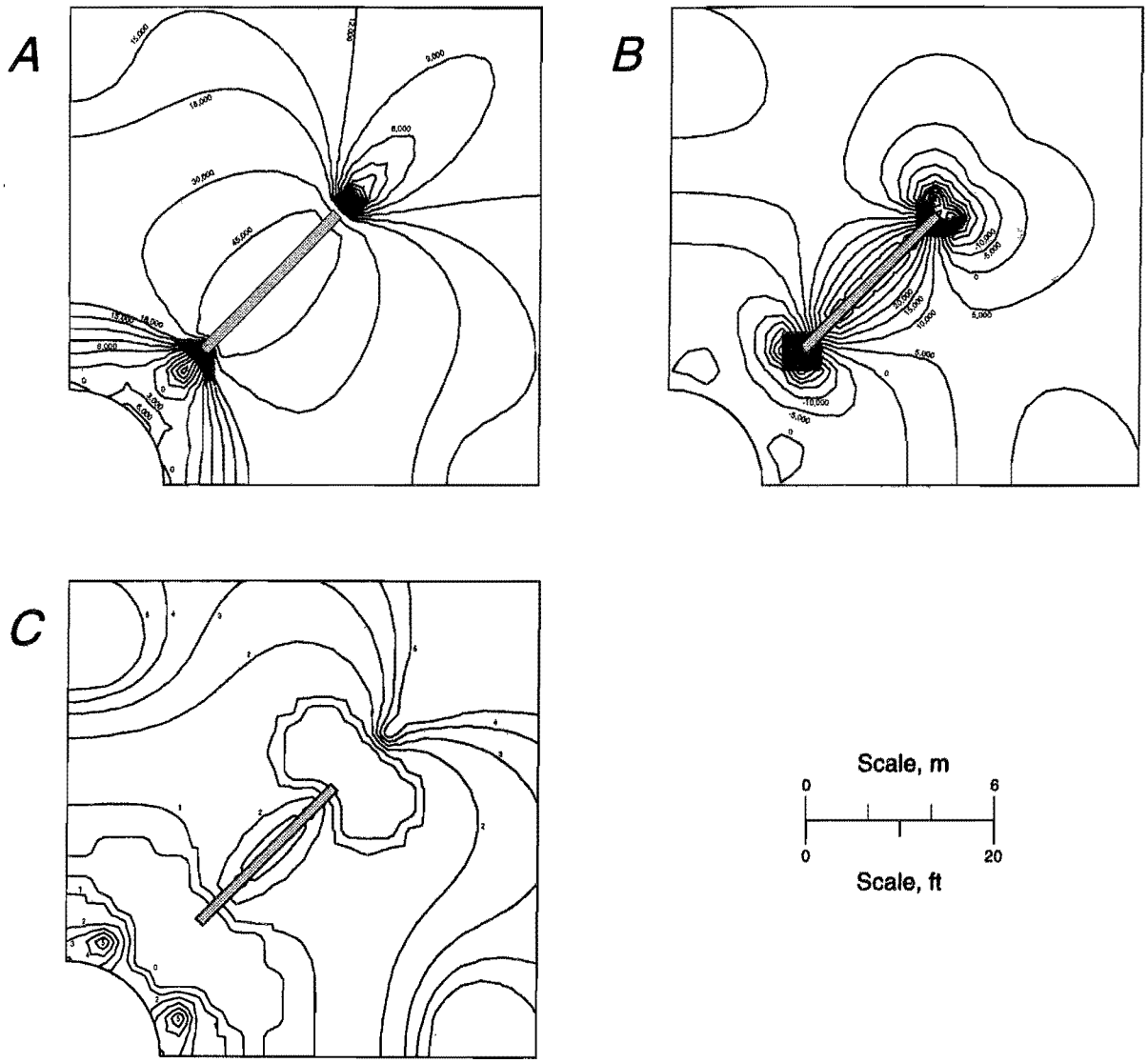


***Slots with 345-MPa (50,000-psi) internal pressure surrounding a circular opening in a hydrostatic stress field. A, Maximum principal stress distribution; B, minimum principal stress distribution; C, strength factor distribution.***

*Figure 12*

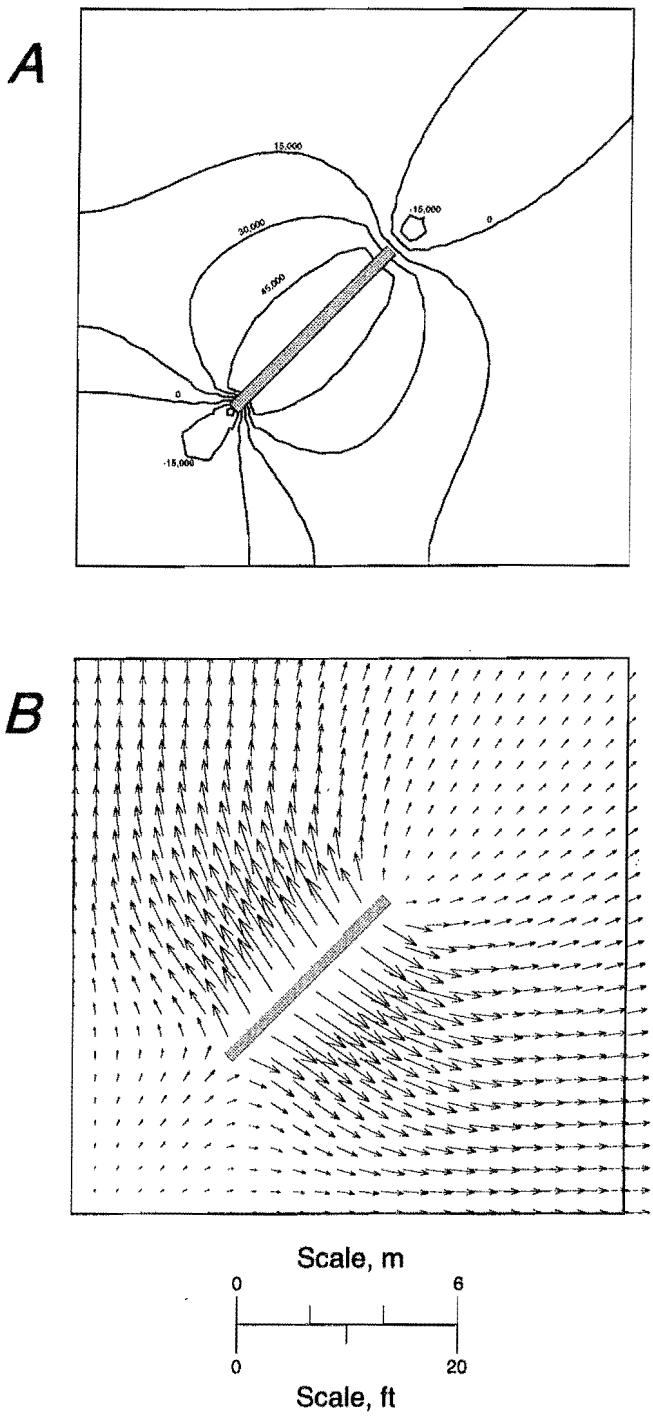


***Slots with 345-MPa (50,000-psi) internal pressure in a model with no opening or field stress. A, Maximum principal stress distribution; B, relative displacement.***

*Figure 13*

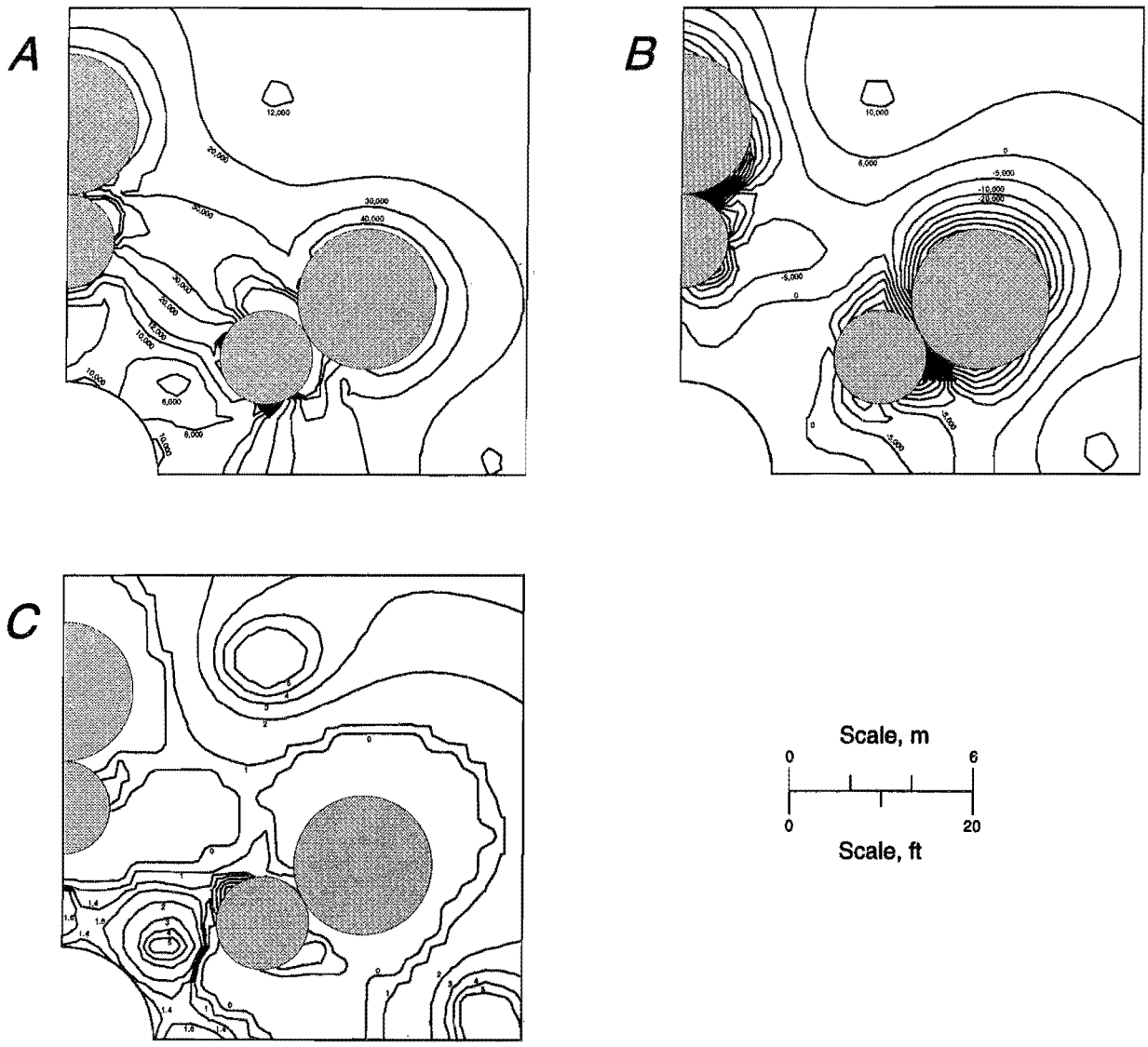


***Double ring of pressure spheres surrounding a circular opening in a hydrostatic stress field. A, Maximum principal stress distribution; B, minimum principal stress distribution; C, strength factor distribution.***

*Figure 14*

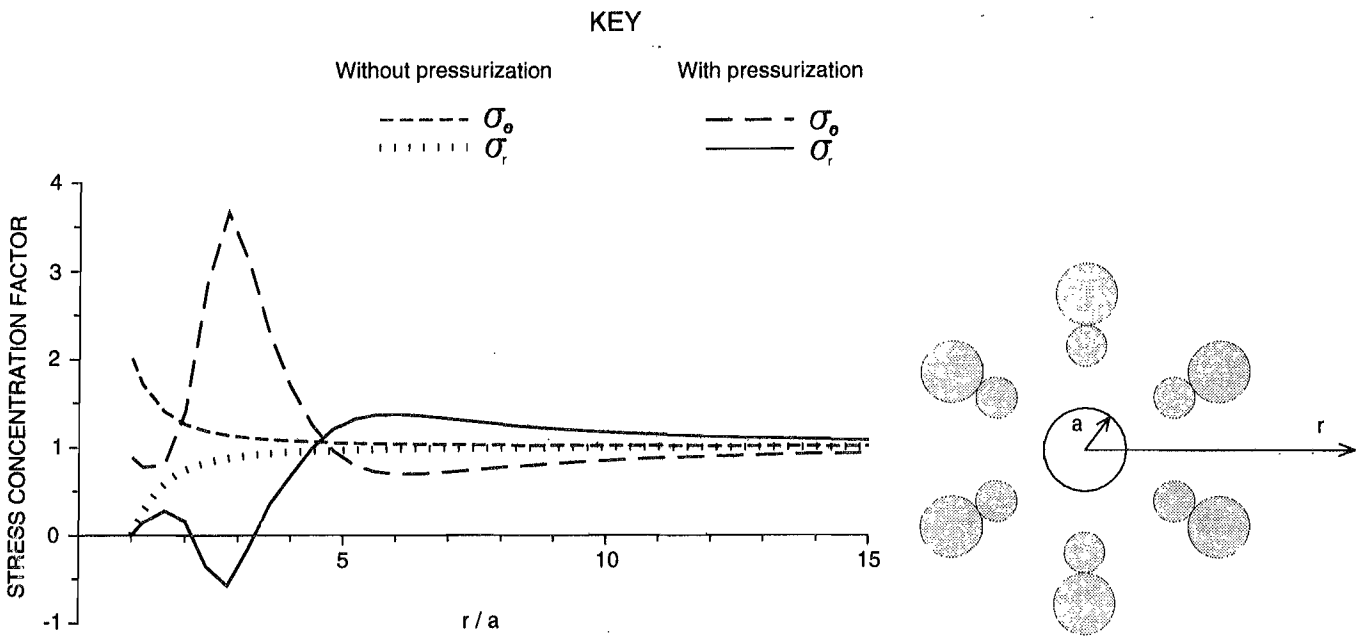


***Radial ($\sigma_r$) and tangential ($\sigma_\theta$) stress distribution near a circular opening in a hydrostatic stress field, with and without pressurization.***

can be concluded that reductions in compressive stress concentrations on the opening surface depend on the relative magnitudes of the tangential and radial stresses induced.

All of the models discussed to this point have incorporated pressure spheres with uniform internal loading. In practice of course, the zones of induced pressure would not be perfectly uniform. To simulate this uneven loading, a model was run in which the normal stress on adjacent sphere elements was randomly varied by ±6.9 MPa (±1,000 psi) (see appendix A, figure A-7). This model resulted in tangential stresses on the opening surface between 34 to 103 MPa (5,000 and 15,000 psi), and strength factors between 1 and 2, which is similar to the result obtained with the idealized spheres. This suggests that the mechanisms associated with rock pressurization can be created under less than ideal conditions.

## PRESSURIZATION APPLIED TO COUNTER THE EFFECTS OF A BIAXIAL STRESS FIELD

The excavations discussed to this point have all been subjected to a hydrostatic stress, ($\sigma_H = \sigma_V$). In many cases, especially at shallower depths, the horizontal stress exceeds the vertical stress (*23*). In these cases, stability problems may arise from the nonuniform stress distribution on the opening surface. To examine the potential of pressurization to produce a more uniform stress distribution, a model was run with $\sigma_H = 3\sigma_V = 69$ MPa (10,000 psi). The maximum principal stress contours in figure 15*A* show that this loading would produce a nonuniform stress distribution on the opening, with higher compressive stresses in the back. The associated distributions of minimum principal stress and relative displacement are shown in figures 15*B* and 15*C*. The high stress concentration in the back leads to a strength factor (figure 15*D*) of less than 1, which indicates probable failure.

To create a more uniform stress distribution on the opening surface, two 3-m (10-ft), 276-MPa (40,000-psi) pressure spheres were placed in the back and floor 7.6 m (25 ft) from the model center. This arrangement results in a more uniform tangential stress distribution on the opening (figure 16*A*). The minimum principal stress distribution in the vicinity of the opening (figure 16*B*) is also more uniform. However, the overall stability of the opening is not greatly improved. Strength factors on the opening surface (figure 16*C*) are in the 1 to 2 range, with failure likely at 0°, 45°, and 90° from horizontal.

By removing the opening and field stress, it can be seen that the spheres increase the vertical stress component (figure 17), thereby decreasing the difference between $\sigma_V$ and $\sigma_H$ in the vicinity of the opening. This results in a principal stress distribution near the opening similar to that associated with hydrostatic loading. Although opening

*Figure 15*

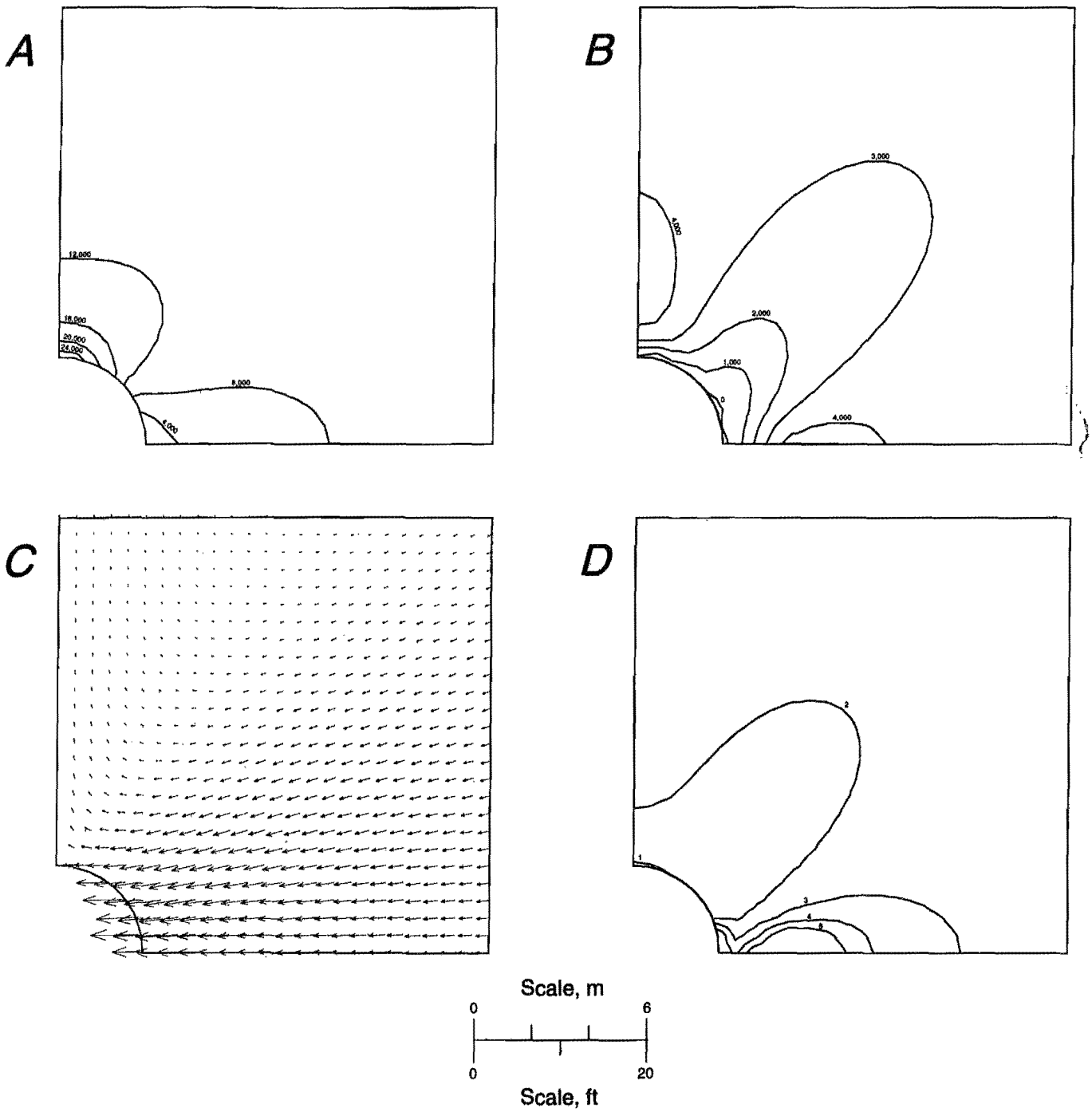


***Circular opening in a biaxial stress field where $\sigma_H = 3\sigma_V$ = 69 MPa (10,000 psi). A, Maximum principal stress distribution; B, minimum principal stress distribution; C, relative displacement; D, strength factor distribution.***

*Figure 16*

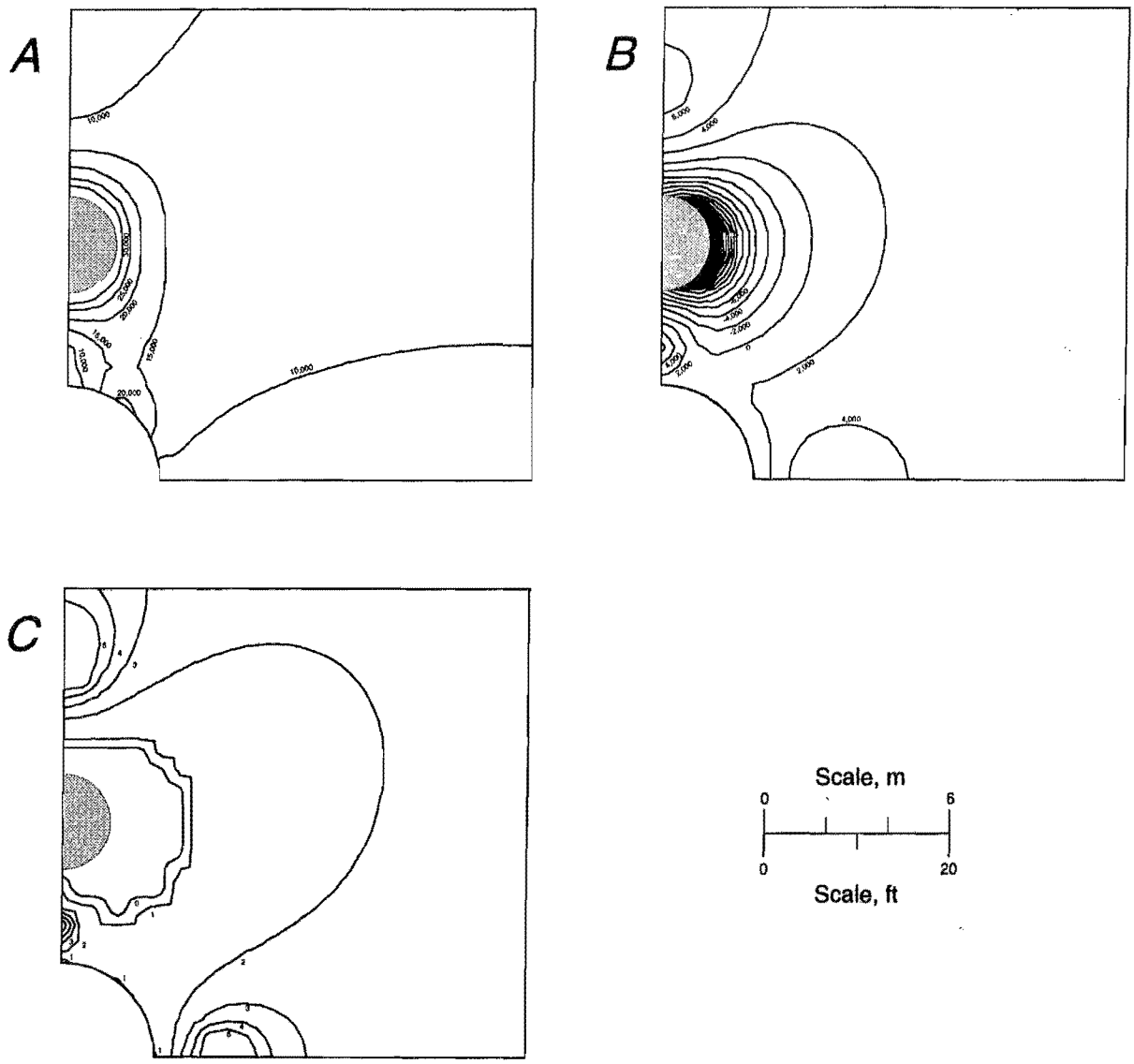


***Spheres with 276-MPa (40,000-psi) internal pressure placed in line with the minimum principal stress direction near an opening in a biaxial stress field. A, Maximum principal stress distribution; B, minimum principal stress distribution; C, strength factor distribution.***

*Figure 17*

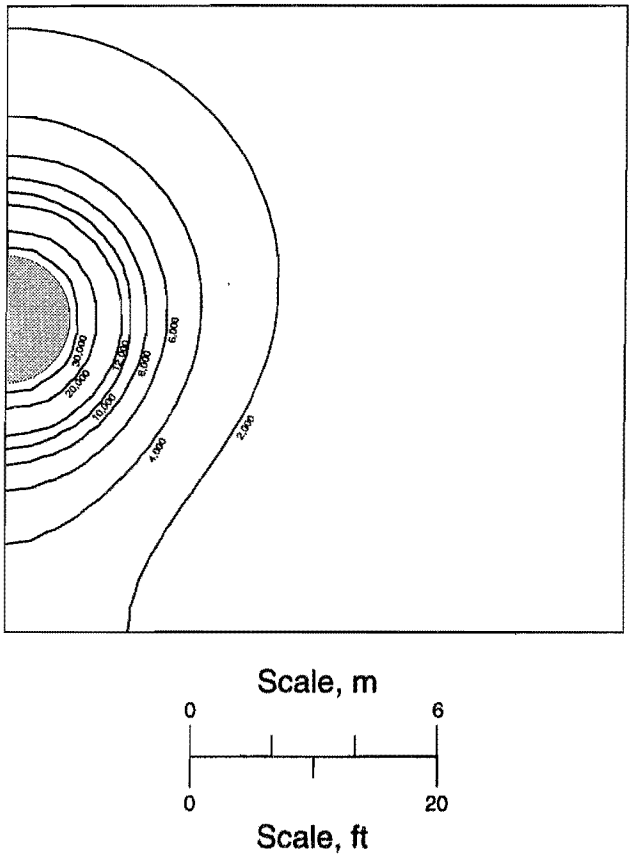


***Spheres with 276-MPa (40,000-psi) internal pressure placed above and below the center of a model with no opening or field stress, maximum principal stress distribution.***

stability was not improved in this particular example, there may be cases where this pressurization application would be useful.

## PRESSURIZATION APPLIED TO INCREASE COMPRESSIVE STRESS ON THE OPENING SURFACE

In special situations, it may be desirable to increase rather than to decrease compressive stress concentrations on the opening surface. A concept under consideration by the Electric Power Research Institute (EPRI) (*24*) is an example. EPRI is examining methods to contain compressed air in underground caverns. The air would be compressed using energy from hydroelectric power plants during hours of low electricity demand. During peak hours, when demand is high, the compressed air would be used to drive turbines for electrical power generation. The problem with this concept is that in order to contain the compressed air, large storage caverns would have to be excavated at depths where the overburden pressure is sufficient to counteract the air pressure. One potential solution to this problem is to induce stresses in the wall rock to counteract the air pressure in the storage cavern. This would allow higher air pressures to be contained in smaller, near-surface caverns. By reducing cavern size and depth, large savings in cavern and shaft construction costs could be realized.

To evaluate the applicability of rock pressurization to this problem, a test case presented by EPRI was modeled. The case is that of a circular tunnel 6.1 m (20 ft) in diameter, 152 m (500 ft) deep, with an operating pressure range of 2.2 to 34 MPa (325 to 5,000 psi). The assumed physical properties of the rock are the same as those of previous models (see appendix A). Using data presented by Hoek (*23*), a horizontal stress of 16 MPa (2,300 psi), 4.2 times the vertical stress, was used. Figure 18*A* shows the maximum principal stress distribution around the cavern. The radial stresses on the opening surface are equal to the 34-MPa (5,000-psi) air pressure within the cavern. The minimum principal stress distribution (figure 18*B*), shows that tangential tensile stresses are induced in the rib of the tunnel. These tensile stresses would cause radial fractures to form in the rib, as indicated by the presence of the failure zone in figure 18*C*.

To counteract the tensile stresses induced by the compressed air, eight 4.6-m (15-ft) pressure spheres were placed 12.2 m (40 ft) from the model center at 45° intervals. To compensate for the biaxial stress field, unequal sphere pressures were used, with the upper and lower sphere pairs pressurized to 345 MPa (50,000 psi) and the left and right sphere pairs pressurized to 276 MPa (40,000 psi). Figures 19*A* and 19*B* show that while the radial stresses on the cavern surface are still about 34 MPa (5,000 psi), tangential stresses near the cavity are now compressive. The pressure spheres create a ring of compressive stress around the cavern, as shown in figure 19*B*, which in turn prevents the formation of tensile fractures. The strength factor distribution (figure 19*C*) indicates that the cavern is stable, with strength factors near the cavern approaching 2. At the low air-pressure extreme of 2.2 MPa (325 psi), cavern stability is maintained (see appendix A, figure A-8).

In addition to ensuring cavern stability, pressurization should tend to close preexisting rock fractures, thereby lowering the air permeability of the rock.

*Figure 18*

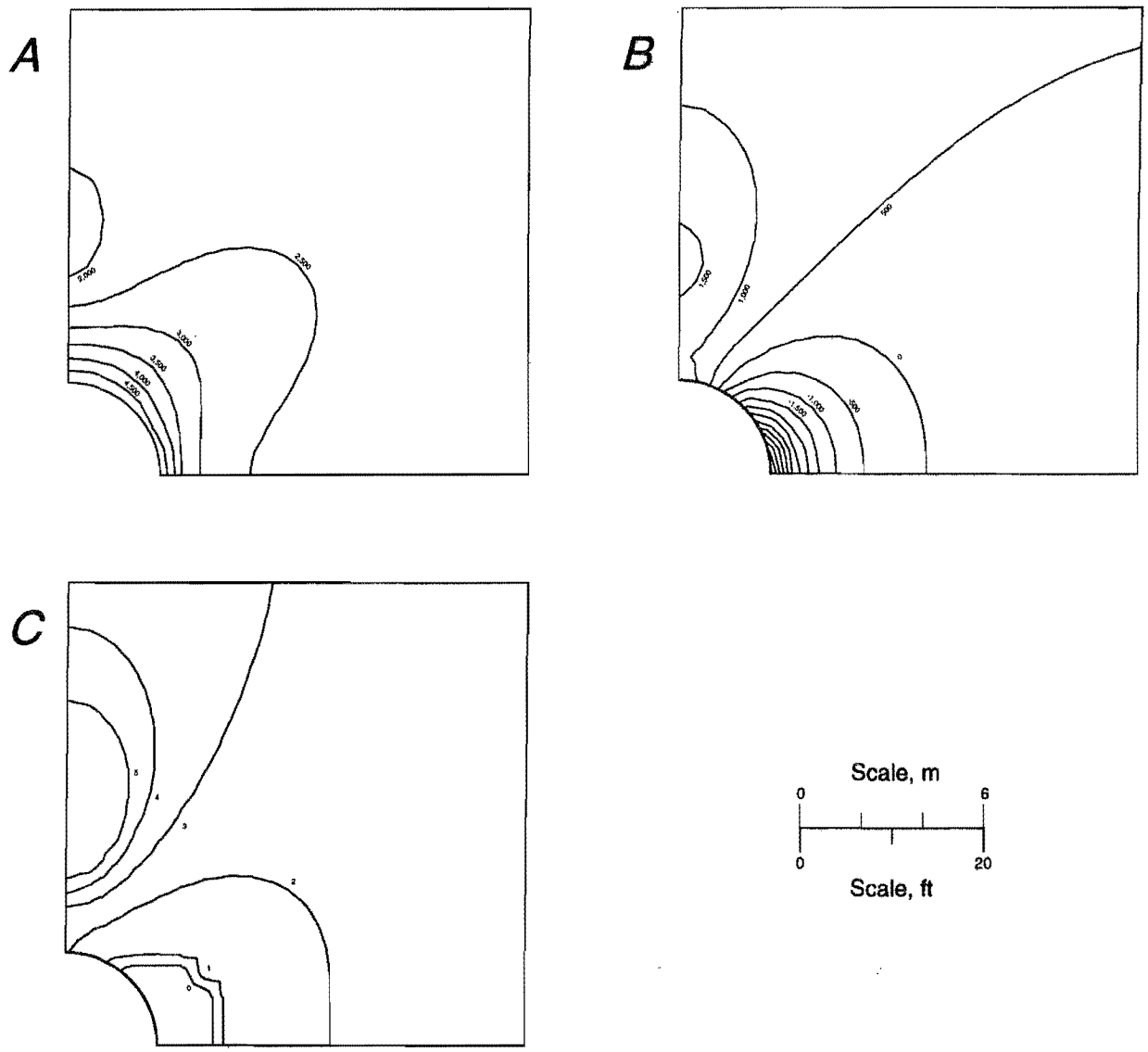


***Circular opening internally loaded with 34-MPa (5,000-psi) air pressure. A, Maximum principal stress distribution; B, minimum principal stress distribution; C, strength factor distribution.***

*Figure 19*

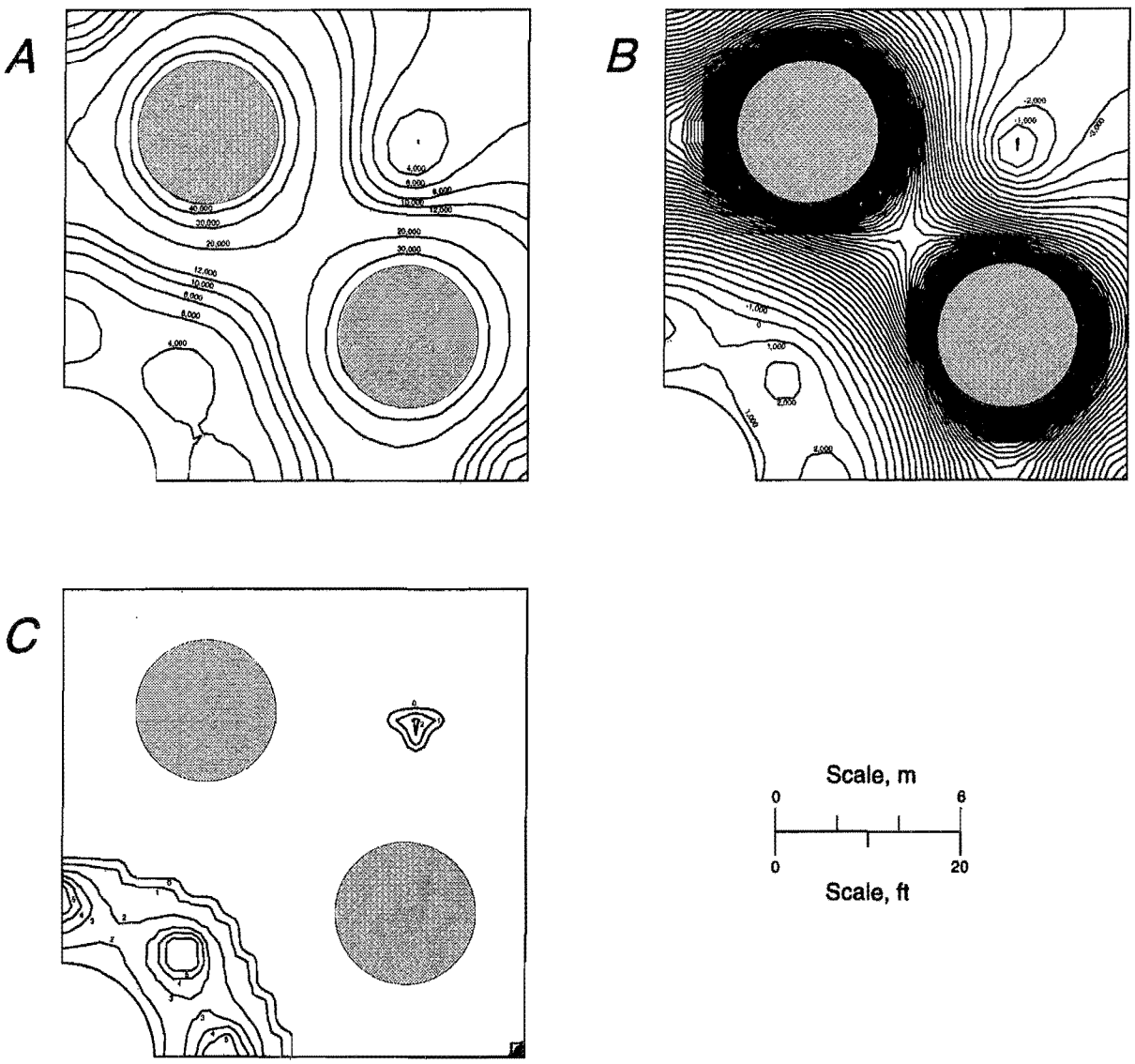


***Single ring of pressure spheres surrounding a circular opening internally loaded with 34-MPa (5,000-psi) air pressure. A, Maximum principal stress distribution; B, minimum principal stress distribution; C, strength factor distribution.***

# LABORATORY EXPERIMENTATION PROGRAM

To investigate practical aspects of the pressurized sphere concept, a series of laboratory experiments was performed. The laboratory work was conducted in two major phases. In the first phase, several unconfined concrete cubes were hydraulically fractured with molten sulfur. These unconfined fracturing tests were performed to evaluate sulfur as a fast-setting, low-cost, injection fluid. To accomplish the fracturing tests, a sulfur injection system was designed, tested, and refined. After demonstrating the feasibility of fracturing with sulfur, the second test phase was conducted by injecting sulfur into a confined concrete cube in order to create reoriented hydraulic fractures. The ultimate goals of the experimentation program were to—

- Demonstrate under controlled laboratory conditions that repeated injection with a settable fluid causes successive fractures to reorient such that a roughly spherical zone of radially oriented compressive stress is induced; and
- Evaluate the validity of the assumptions used in the boundary-element analysis by gathering data on fracture orientation, radius, width, volume, and extension pressure.

## FRACTURING FLUID SELECTION

The process of pressure sphere formation through repeated hydraulic fracturing with a settable fluid requires a fluid that can be pumped at pressures sufficient to initiate and fill fractures in the rock mass. To control the extent of the fracture, the fluid is required to flow into the fracture and quickly set after a small volume has been injected. The phase change from a pumpable, low-viscosity fluid to a solid can be driven by two basic phenomena: chemical reaction and temperature change.

After careful consideration of chemical grouting systems, including two-shot (*25*) and in-hole mixing systems (*26*), several reasons emerged for eliminating chemical reaction as a means of solidification. First, chemical grouts would require separate high-pressure pumping systems. Secondly, it was anticipated that mixing multiple components within a borehole at the pressures necessary to initiate hydraulic fracture would be very difficult. Another drawback was the possibility of grout accidentally setting within the injection system; this would result in major damage to the system.

Considering the difficulties associated with chemical grouting systems, a heated injection system was chosen for the laboratory tests. Heated systems use molten grout that sets as it cools. Although uncommon, heated grouting systems date to at least 1919, when tar was used to fill fractures and reduce leakage around a dam in Tennessee (*27*). Sulfur was chosen as the injection fluid because it has a low melting point (119 °C [246 °F]), is pumpable, noncorrosive, and relatively inexpensive; the 1990 price of sulfur was less than 9 cents per kilogram (4 cents per pound) (*28*).

In examining sulfur as a fracturing fluid, the primary issues of concern are its melting point, its viscosity, and the manner in which it solidifies. Sulfur has two stable crystalline forms, rhombic ($S_\alpha$) and monoclinic ($S_\beta$), with differing phase characteristics (*29*). Rhombic sulfur is the stable form at temperatures below 96 °C (204 °F). Monoclinic sulfur is stable between 96 °C (204 °F) and the melting point of 119 °C (246 °F). Because rhombic sulfur turns into monoclinic very slowly, it is possible to melt rhombic sulfur directly, in which case the melting point is 113 °C (235 °F). Pressure has only a small effect on the melting point, as shown in the generalized phase diagram for sulfur (figure 20).

In the liquid state, sulfur viscosity drops with rising temperature, up to about 160 °C (320 °F) (figure 21). Above this temperature, there is an anomalous increase in viscosity. At about 188 °C (370 °F) the viscosity reaches a maximum and molten sulfur barely flows. As the temperature rises further, the viscosity once again drops. Sulfur will ignite between 246 and 266 °C (475 and 510 °F), and will boil at 444 °C (832 °F) (at atmospheric pressure).

The viscosity spike associated with sulfur is, of course, detrimental to pumping. Fortunately, many substances can be used to lower sulfur viscosity, including iodine, bromine, chlorine, and organic materials (*30*). In fact, commercial-grade sulfur usually contains sufficient amounts of organic contaminants to eliminate, for practical purposes, the viscosity spike. The commercial-grade sulfur used in the laboratory experiments proved to have enough impurities to be readily pumpable.

When cooled, sulfur decreases in volume approximately 15%. During solidification, this volume decrease would result in a decrease in induced stress perpendicular to the fracture plane; however, this could be compensated for by increasing the number of fracturing cycles. If sulfur is quickly cooled from temperatures above 160 °C (320 °F) to room temperature, a rubber-like mass containing a large proportion of amorphous sulfur is formed. This supercooled sulfur will remain rubber-like for a period of days. The unconfined cube tests were designed in part to investigate the possibility that amorphous sulfur would form as the fluid contacts the walls of an induced fracture.

## HYDRAULIC FRACTURING PROCESS

The assumption that roughly spherical zones of high pressure can be formed by repeated hydraulic fracturing with a settable fluid is based on hydraulic fracturing

*Figure 20*

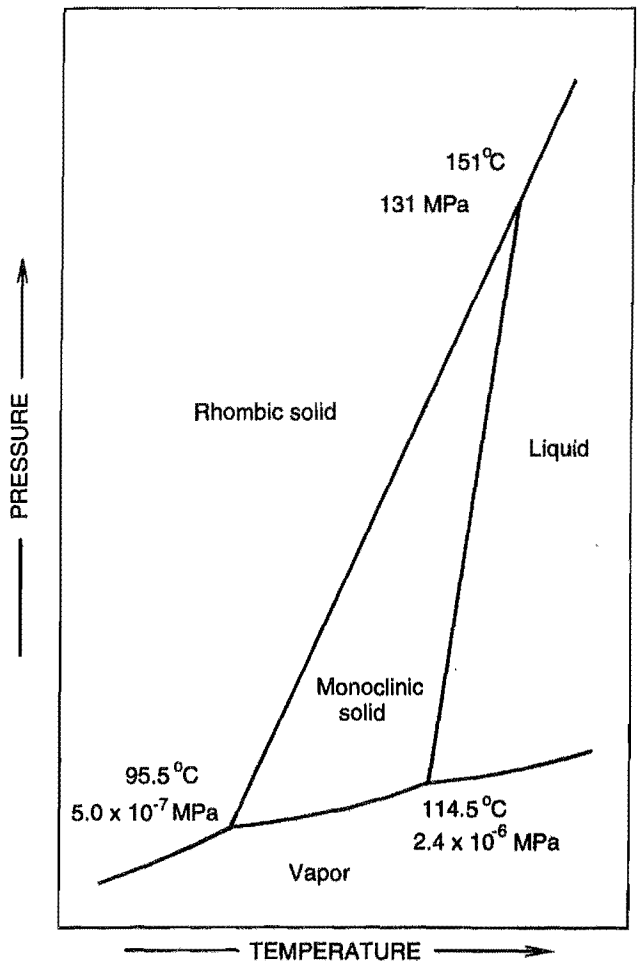


***Generalized sulfur phase diagram. Source: Freeport Sulphur Company.***

*Figure 21*

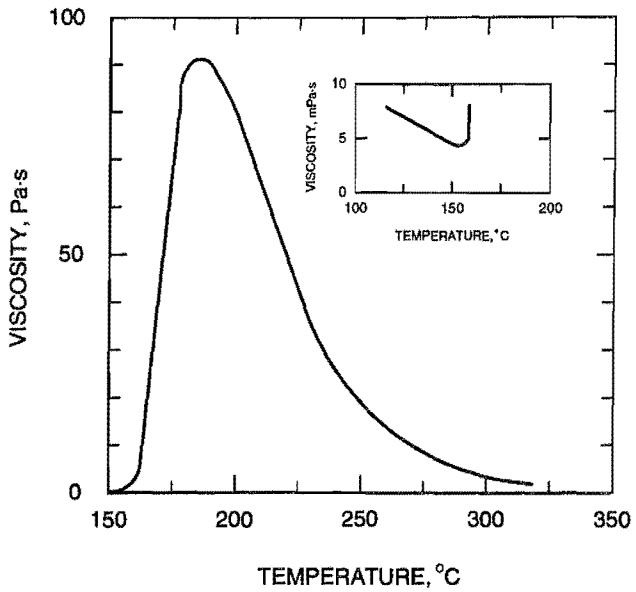


***Sulfur viscosity as a function of temperature. Source: Freeport Sulphur Company.***

research performed in the petroleum industry. To design appropriate laboratory tests of the pressurized sphere concept, the fundamentals of hydraulic fracture initiation from a packed-off borehole were reviewed and are briefly summarized here. A more detailed discussion appears in appendix B.

Hydraulic fracturing, the process of initiating and extending rock fractures by pressurized fluid injection, was first introduced in 1947 as a means of stimulating gas well production (*31*). In those early years, it was assumed that hydraulic fractures were created and extended along bedding planes. However, theoretical and experimental work quickly showed that the stress field in the vicinity of the fracture is the major control on fracture orientation, with fractures propagating perpendicular to the least compressive principal stress. This observation is central to the pressurized sphere concept. By using a settable fracturing fluid to "lock in" the compressive stresses induced perpendicular to the fracture plane, the local minimum principal stress direction is rotated, and subsequent fractures open up perpendicular to this direction.

The process of repeated, reoriented hydraulic fracturing begins with fracture initiation or extension. Fracturing will be initiated or existing fractures will be extended from a packed-off borehole when the fluid pressure in the borehole reaches a critical value (*32*). In dry, impermeable rock this value is:

$$P_c = \sigma_t + 3\sigma_3 - \sigma_2, \qquad (1)$$

where $P_c$ = critical pressure,

$\sigma_t$ = rock tensile strength,

$\sigma_3$ = minimum principal stress in the plane perpendicular to the borehole axis,

and $\sigma_2$ = maximum principal stress in the plane perpendicular to the borehole axis.

When the critical pressure is reached, fractures are initiated or extended perpendicular to the minimum principal stress ($\sigma_3$) direction. If a settable fracturing fluid such as sulfur is used, the filled fractures induce compressive stresses normal to their surface, in the direction of $\sigma_3$.

The following example illustrates the envisioned repeated fracturing process. Suppose a dry, intact, confined concrete block ($\sigma_t$ = 3.4 MPa [500 psi]) with no external loading is to be fractured with sulfur from a borehole along the z axis. The initial stress state is $\sigma_x = \sigma_y = \sigma_z = 0$. From equation 1, the predicted critical pressure is $P_c = 3.4 + 3(0) - 0 = 3.4$ MPa (500 psi). Assume that fracturing occurs in the y-z plane and that a compressive stress of 2.9 MPa (425 psi) is maintained in the x direction due to the sulfur-filled fracture. After solidification, the idealized stress state in the block is now $\sigma_x$ = 2.9 MPa (425 psi), $\sigma_y = \sigma_z = 0$. For the second injection, the critical pressure would be $P_c = 3.4 + 3(0) - 2.9 = 0.5$ MPa (75 psi). Assuming the second fracture occurred in the x-z plane, and that 0.4 MPa (65 psi) of induced stress is maintained, the new stress state would be $\sigma_x$ = 2.9 MPa (425 psi), $\sigma_y$ = 0.4 MPa (65 psi), $\sigma_z = 0$. The third injection would probably induce fracturing along the z axis at some angle between the x and y planes. The pressure required to induce this fracture would be $P_c = 3.4 + 3(0.4) - 2.9 = 1.7$ MPa (270 psi). The stress distribution actually induced by fracturing would, of course, be more complex, but this idealized example serves to illustrate how the repeated fracturing process might progress.

## TEST APPARATUS

High pressures and temperatures are required to fracture with sulfur. To accomplish this, an injection system consisting of a high-pressure sulfur pump and a heated packer assembly was designed. This injection system was used for both the confined and unconfined fracturing tests. In addition, a confining frame was designed for use in the confined block tests.

### Sulfur Pump and Packer Assembly

A pump capable of delivering molten sulfur at 41 MPa (6,000 psi) and 204 °C (400 °F) was designed and fabricated. Major components of the closed-loop pumping system (figures 22 and 23) include a sulfur reservoir, a positive-displacement piston pump driven by a pneumatic motor, and a relief valve. All components through which sulfur flows are individually heated and connected by heated stainless steel tubing (0.635-cm [0.250-in] outside diameter [OD], 0.478 cm [0.188-in] inside diameter [ID]). Temperature throughout the system is monitored using thermocouples; heaters are individually controlled so that all components can be maintained at temperatures between 149 and 204 °C (300 and 400 °F).

A mechanical packer assembly was designed to form a 41-MPa (6,000-psi) seal against the concrete wall of the borehole while heating a sulfur pool at the injection point to temperatures in excess of 149 °C (300 °F). The packer assembly (figures 22 and 24) is contained in a 3.18-cm- (1.25-in-) OD packer body made of stainless steel. The

*Figure 22*

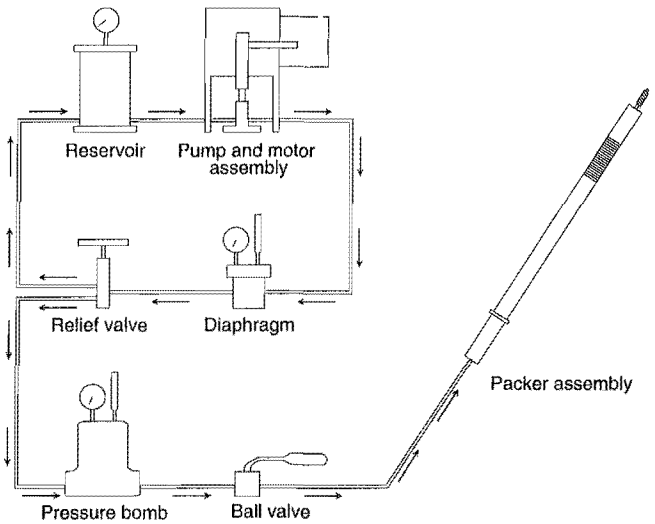


***Injection system schematic, showing direction of sulfur flow.***

*Figure 23*

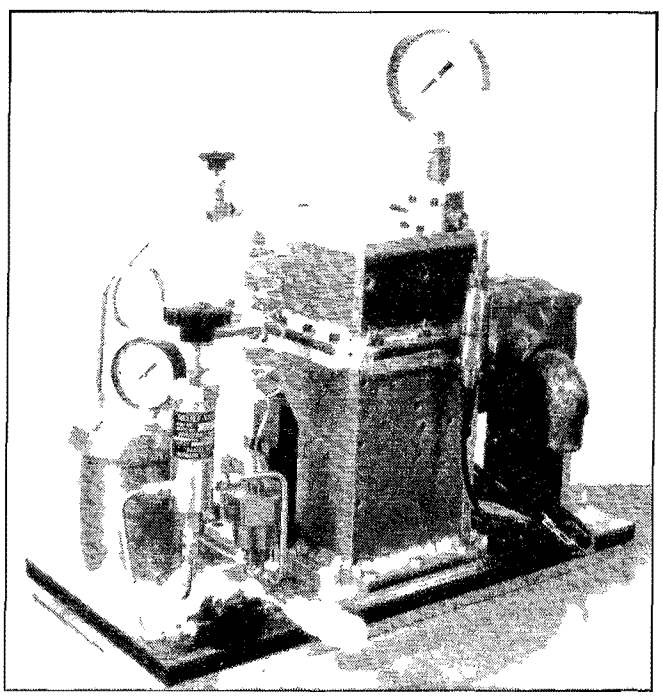

***Sulfur pumping system.***

*Figure 24*

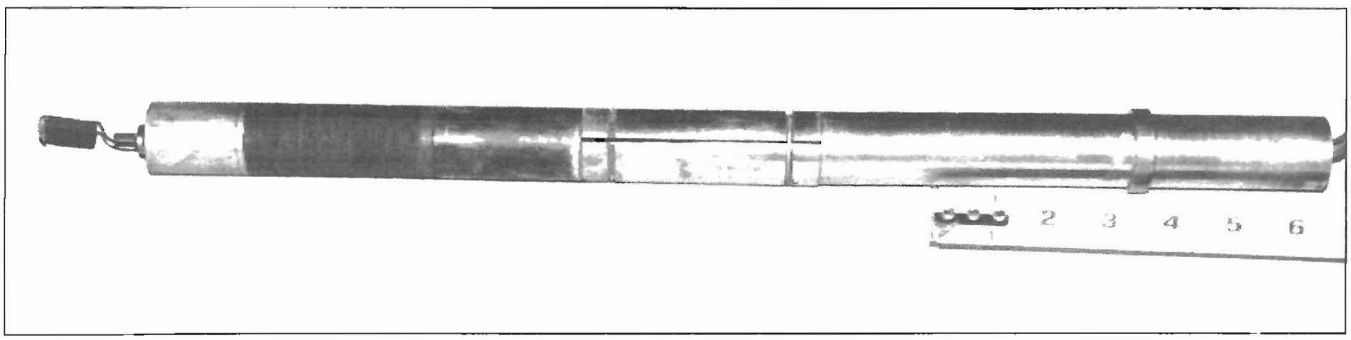

*Packer assembly.*

inner diameter of the packer body contains a 0.160-cm (0.063-in) electric cable heater, and a 0.318-cm (0.125-in) sulfur injection tube. The cable heater is fastened to the sulfur injection tube to keep sulfur within the tube molten. This heater also passes through the head of the packer assembly to maintain a pool of molten sulfur at the point of injection. A chromel-alumel thermocouple embedded in the concrete block is used to monitor pool temperature.

### Confining Frame

To create multiple, reoriented hydraulic fractures, the material being fractured must be confined. Underground, confinement is provided by the surrounding rock. In the laboratory, a similar confinement was provided to the test specimen by means of a confining frame. The frame (figure 25) consists of six 1.91-cm-thick (0.75-in-thick) aluminum plates that form a cube 61 cm (24 in) on a side. Each plate is backed by three 10.2-cm by 10.2-cm (4-in by 4-in) steel I-beams. Opposite sides of the frame are connected and held together by twelve 2.54-cm-diam (1-in-diam) threaded rods with nuts. In order to assemble the frame, the 36 rods pass through holes drilled in the webs of the I-beams.

The aluminum plates serve two purposes. First, they comprise a form for casting a 57.2-cm (22.5-in) concrete test cube. Later, during fracturing, they provide a uniform confinement for the loads generated within the test block. The I-beams serve to back up the plates and provide a linkage between the plates and the steel rods. The steel rods are tensioned by the loads generated during fracturing.

Based on an allowable rod load of 200 kN (45,000 lbf), the maximum confinement provided by the frame was calculated as:

*Figure 25*

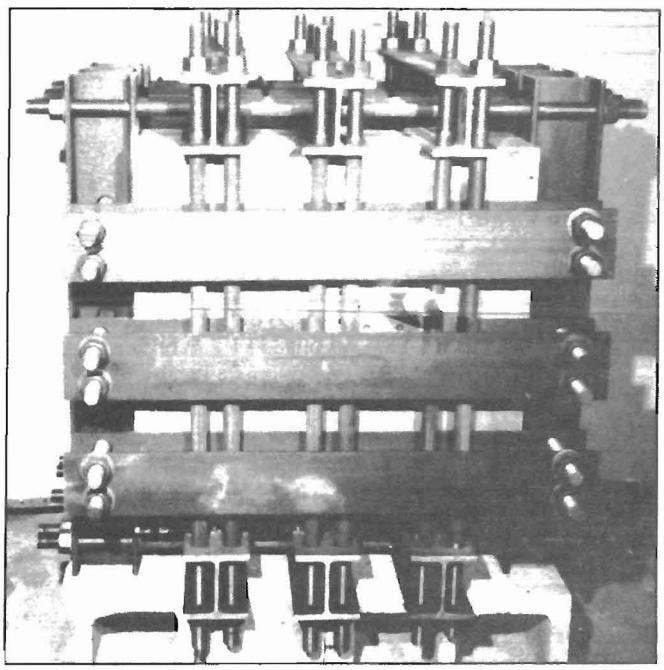

*Confining frame.*

$$(200 \text{ kN/rod} \times 12 \text{ rods})/(57.2 \text{ cm})^2$$

$$= 7.3 \text{ MPa } (1{,}100 \text{ psi}).$$

Because loads generated in the block are carried by the steel rods, fracture pressure and orientation can be estimated by measuring rod loads in each of the three orthogonal directions. To measure rod loads, load cells were placed between the rod nut and the I-beam on opposite ends of opposing center-rod pairs (figure 26).

*Figure 26*

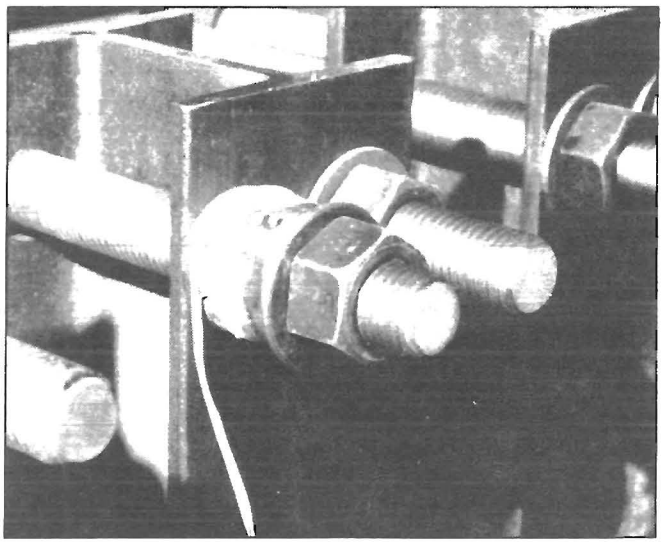

*Load cell used to measure confining frame rod load.*

## EXPERIMENTATION PROCEDURE AND RESULTS

### Unconfined Fracturing Tests

Samples for unconfined fracturing tests were prepared by embedding heated injection tubes in 0.3-m (1-ft) concrete cubes. Prior to embedding the tubes in concrete, a simulated borehole was created at the injection tube outlet by casting a 3.18-cm-diam (1.25-in-diam) wax plug around the outlet. To study the effects of borehole length/diameter (L/D) ratio on fracturing pressure, different plug lengths were used for different samples. To heat the injection tubes and to provide for a molten pool at the point of injection, a 0.318-cm-diam (0.125-in-diam) cable heater was attached along the length of the injection tube and coiled within the wax plug. A thermocouple was also embedded in the plug to monitor injection point temperature. The wax plug was then centered in a plywood form, and concrete with a 1.25:1 sand-cement ratio was poured around the plug and injection tube. Five samples were poured in this manner. To perform a fracturing test using the packer assembly, one sample was poured around a 3.18-cm-diam (1.25-in-diam) aluminum plug. After the sample cured, the plug was removed, leaving a 3.18-cm (1.25-in) borehole.

Twenty 5-cm-diam (2-in-diam) cylindrical samples were cast from this pour and later tested to determine the strength properties of the blocks. The average compressive and tensile strengths were 72 MPa and 3.1 MPa (10,400 psi and 450 psi), respectively.

From the outset, difficulties were encountered in the unconfined fracturing tests. One of the main shortcomings was that injection pool pressures could not be directly monitored. Instead, it was assumed that the system pressure and the pool pressure within the block equalized when the ball valve was opened. This assumption is not valid if a blockage exists between the pressure monitoring point of the system and the sulfur pool.

The first unconfined fracturing test was performed on the block with an injection point L/D ratio of 1:1. Initially, the block did not fracture, even with the system pressure at its maximum of 41 MPa (6,000 psi). This was probably because of a blockage at some point in the system between the pressure transducer and the injection point. The blockage eventually must have been cleared, because the block unexpectedly fractured as the experiment was being shut down. By this time, the data logger had been shut off, and the fracturing pressure was not recorded. The block fractured with the long axis of the embedded tube in the fracture plane (figure 27). This orientation was observed in all subsequent fracturing tests. The sulfur on the fracture surface hardened quickly, suggesting that the formation of supercooled, amorphous sulfur may not be a problem.

Of the original six blocks cast, the only quantitative fracturing data came from the block cast around the aluminum plug. To test this block, the packer assembly was inserted in the borehole to leave a cylindrical void with a L/D ratio of 0.2:1 at the tip of the assembly. The packer was then set, and sulfur was injected under increasing pressure until fracturing occurred along the packer axis (figure 28), at a pressure of 34.3 MPa (4,980 psi).

In an attempt to overcome the supposed problems of sulfur blockage, three additional 0.3-m (1-ft) cubes were cast using wax plugs with L/D ratios of 0.4:1, 0.6:1, and 0.8:1. These blocks featured a capped outlet line from the injection pool. If blockage problems arose, the cap could be removed to check sulfur flow through the test block. As with the first set of cubes, 20 cylindrical samples were cast and tested to determine the strengths of these blocks. The average compressive and tensile strengths of these samples were 50 MPa and 2.7 MPa (7,270 psi and 390 psi), respectively.

The second set of blocks were fractured with only minor difficulty. A summary of the unconfined fracturing tests appears in table 1.

The fracturing pressures for the four successful fracturing tests are plotted against L/D ratio on figure 29. From the curve fitted to these data points, it is inferred that for L/D ratios higher than 1.1, tensile strength, rather than borehole geometry, is the control on fracturing pressure for these tests.

Table 1.—Summary of unconfined fracturing test results

| Block | L/D | Result |
|---|---|---|
| | | $\sigma_c$ = 72 MPa (10,400 psi); $\sigma_t$ = 3.1 MPa (450 psi) |
| 1 . . . | 1.0:1 | Fractured unexpectedly with datalogger off; no data taken. |
| 2 . . . | 0.5:1 | Sulfur leaked around injection tube, pressures developed were insufficient to fracture block. |
| 3 . . . | 0.2:1 | Cap poured on top of block to prevent leakage, block fractured at cap/block interface. |
| 4 . . . | 0.2:1 | Fractured at 34.2 MPa (4,980 psi) using packer assembly. |
| 5 . . . | 1:1 | Not tested. |
| 6 . . . | 0.5:1 | Do. |
| | | $\sigma_c$ = 50 MPa (7,270 psi); $\sigma_t$ = 2.7 MPa (390 psi) |
| 7 . . . | 0.4:1 | Fractured at 21 MPa (3,030 psi). |
| 8 . . . | 0.6:1 | Fractured at 14 MPa (2,060 psi). |
| 9 . . . | 0.8:1 | Fractured at 8.6 MPa (1,250 psi). |

L/D Length-diameter ratio.
$\sigma_c$ Compressive strength.
$\sigma_t$ Tensile strength.

## Confined Fracturing Tests

The specimen for confined fracturing tests was made by casting a 57.2-cm (22.5-in) concrete cube around a 3.18-cm-diam (1.25-in-diam) aluminum plug (figure 30). An aluminum guide mounted on the outside of the front confining plate held the plug in position. The angle of the guide ensured that the tip of the plug was centered in the block. After the block had cured, the plug was removed, leaving a borehole for access to the block center. The borehole created in this manner was 6.35 cm (2.5 in) longer than the packer assembly, leaving a void with a L/D ratio of 2:1 for sulfur injection. Based on the unconfined fracturing tests, it was assumed that this L/D ratio would be sufficiently large to allow concrete tensile strength, rather than hole geometry, to control the initial fracturing pressure.

Cylindrical samples from the block pour were tested in the manner previously described to determine the compressive and tensile strength of the block. The compressive and tensile strengths of these samples were 57 MPa and 2.6 MPa (8,240 psi and 380 psi), respectively.

In preparation for each confined fracturing test, the nuts on the threaded steel bars holding the confining frame were tightened to 6.8 N·m (5 ft·lb) of torque. This produced a load in the steel bars, as measured by the load cells, of about 670 N (150 lbf). This bar loading amounts to a nominal triaxial loading on the block of less than 28 kPa (4 psi). After the nuts were tightened, the packer assembly was inserted in the borehole and the packer was set. A cap was placed over the packer assembly and threaded on the aluminum guide. This held the packer assembly in place and ensured that it could not move out of the borehole under pressure. The injection system and packer assembly were then brought up to temperature, and attempts to inject sulfur under pressures of up to 41 MPa (6,000 psi) were made.

*Figure 27*

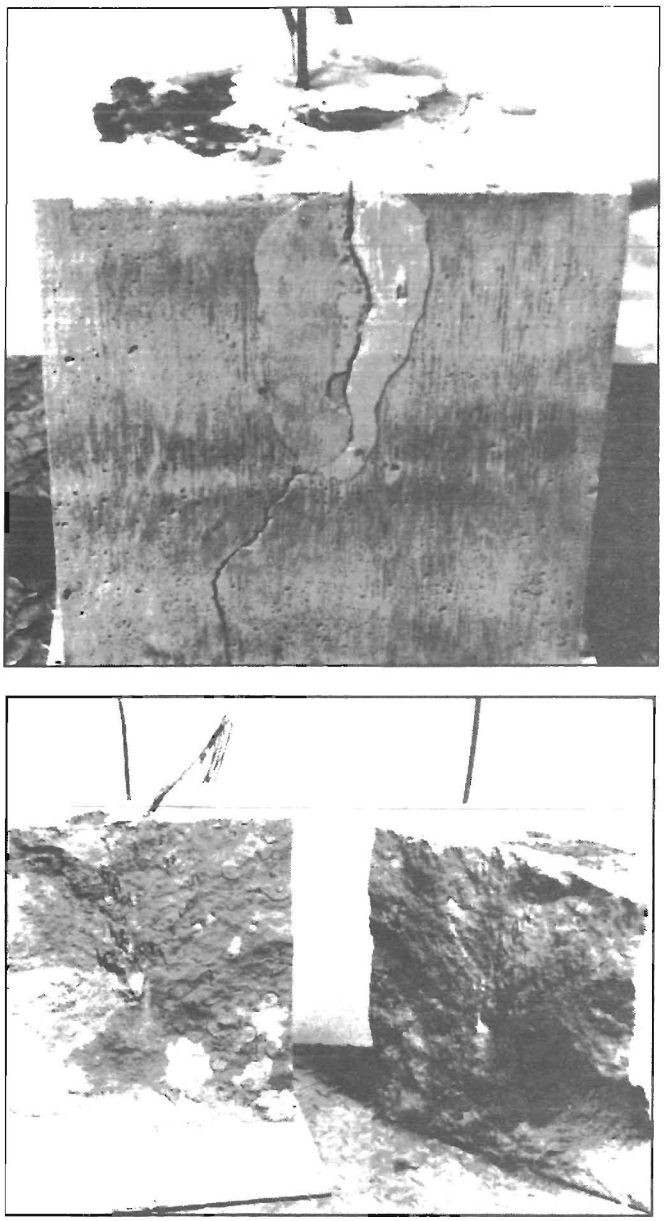

***Block fractured using the embedded pressure tube arrangement (top). Fracture surface exposed by separating block halves (bottom).***

Injection was attempted on eight separate occasions. Component failure plagued the testing effort, with combinations of ball valve, diaphragm, and pump failure occurring during five of the eight injection attempts. The block was not fractured in any of the attempts, despite the fact that sulfur pressures of 41 MPa (6,000 psi) were attained in five of the tests. In each of the tests, the temperature at the injection point was well above the melting point of sulfur.

The exact reason for the failure of the confined fracturing tests is not known, although it seems likely that some blockage existed between the pressure transducer and the point of injection. To verify that the block could be fractured at a pressure below 41 MPa (6,000 psi), an attempt was made to fracture the block using hydraulic fluid. This test was successful, with the block fracturing at a pressure of 8.9 MPa (1,285 psi). It was expected that the block would fracture at a value closer to the tensile strength of the concrete, considering the 2:1 L/D ratio of pressurized borehole.

*Figure 28*

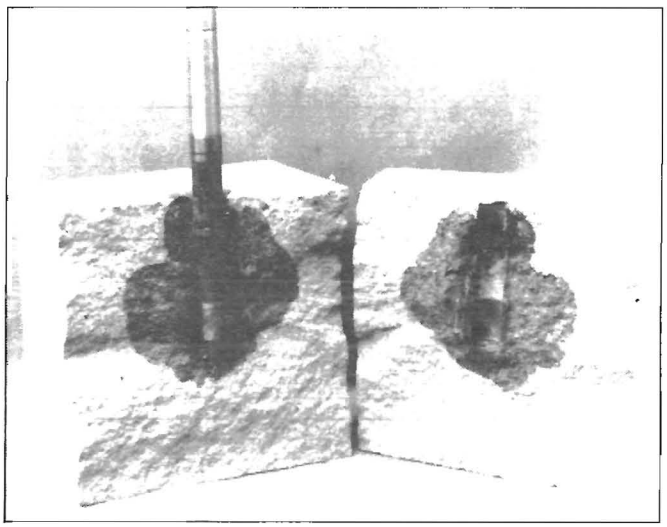

***Block fractured using the packer assembly.***

*Figure 29*

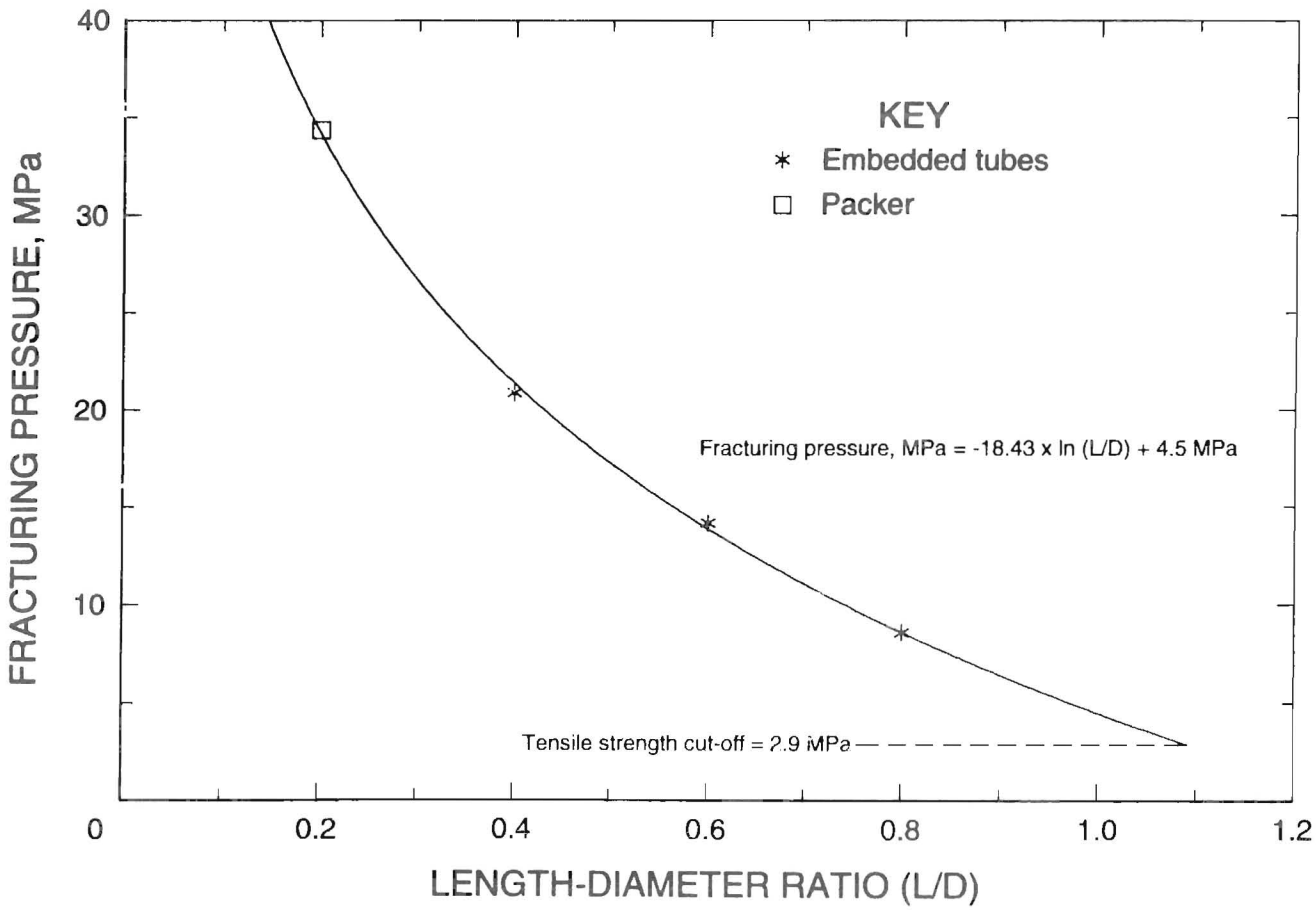


***Fracturing pressure versus L/D ratio for the unconfined fracturing tests.***

*Figure 30*

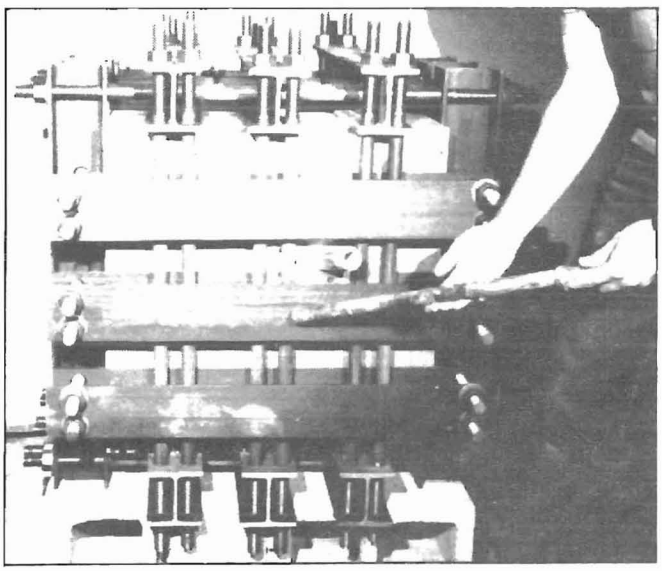

*Aluminum plug used to create access to the confined concrete test block.*

The fracturing test results were, in general, disappointing. The task of building a robust injection system capable of pumping molten sulfur at 204 °C (400 °F) and 41 MPa (6,000 psi) proved difficult. In addition to problems with the ball valve, diaphragm, and pump, blockages in the line between the pressure transducer and injection point were particularly troublesome, although the existence of these blockages can only be inferred due to the lack of direct injection-pool pressure measurements.

There are three basic explanations for blockages in the 0.318-cm-diam (0.125-in-diam) tube between the pressure transducer and the injection point. The first two, that sulfur cooled and solidified in the tube or that a contaminant lodged in the tube, are considered unlikely. During injection, both line and pool temperature were maintained well above the melting point of sulfur. On several occasions during the laboratory work, sulfur was pumped freely through the injection tube and out of the system, with no indication of blockage.

A third explanation is that viscosity changes under high temperature and pressure created a large pressure drop between the pressure transducer and the injection point. To investigate this possibility, the pressure drop in the 0.152-cm- (0.060-in-) ID injection tube was calculated using the Fanning friction factor (*33*). The pressure drop in the tube was found to be a linear function of sulfur viscosity, with

$$\text{Pressure drop, MPa} = 20.3 \times \text{sulfur viscosity, mPa·s.}$$

So, an increase in sulfur viscosity from 0.05 mPa·s to 2.0 mPa·s (0.05 cP to 2.0 cP) would be sufficient to create a 40.7-MPa (5,900-psi) back pressure in the system. In comparison, the pressure drop in the main system tube (0.635-cm [0.250-in] OD, 0.478-cm [0.188-in] ID) for a sulfur viscosity of 2.0 mPa·s (2.0 cP) would only be 0.4 MPa (60 psi).

The 0.318-cm (0.125-in) stainless steel, sulfur injection tube used in the fracturing experiments was chosen for its flexibility, after ensuring that molten sulfur could be pumped through it easily. In retrospect, it appears that a tube with a larger inside diameter should have been used to reduce back pressures caused by viscosity changes under high pressure.

## SUMMARY AND CONCLUSIONS

To significantly increase the stability of underground excavations, methods must be developed to actively control the distribution of stress in the wall rock. By controlling the magnitude and location of stresses around the excavation, the advantages of confined rock strength can be exploited. Past attempts at managing stress by varying excavation geometry and rock support capacity have been adequate in certain situations; however, these techniques are passive in that they only offer limited control of the magnitude and location of stresses within the underground structure.

Active control of the underground stress distribution can be gained by inducing enhanced compressive stresses of known magnitude at specific locations around the excavation. Several methods of accomplishing this have been proposed; Colgate's pressurized sphere concept was chosen for study in this investigation because of its potential for practical field application. Rock pressurization using the pressurized sphere concept involves the creation of roughly spherical zones of radially oriented compressive stress by repeated hydraulic fracturing with a settable fluid. In theory, repeated fracturing with a settable fluid "locks in" induced compressive stresses normal to the plane of fracture and causes subsequent fractures to be reoriented with respect to the inherent, minimum principal stress direction.

The objectives of this investigation were to explore theoretical and practical aspects of rock pressurization and to evaluate its potential as a method of active stress control for underground excavation. The investigation was conducted in two major phases. Numerical modeling

analyses were performed to demonstrate specific applications of rock pressurization, to determine its underlying mechanisms, and to evaluate how different pressurization variables affect the induced stress distribution. Laboratory experiments were performed in an attempt to create a pressurized sphere under controlled conditions and to verify assumptions of the numerical modeling analysis.

Results of the numerical modeling analysis reinforce the assertion that rock pressurization can be used to improve opening stability while exploiting confined rock strength. Specifically, the numerical modeling analysis revealed the following:

1. Circular openings with internal hydrostatic loading can be used to model pressure spheres formed by sequential, reoriented hydraulic fracturing.
2. A single ring of pressurized spheres around the opening increases the tangential stress concentration on the opening surface. The increase in tangential stress concentration is directly proportional to sphere pressure and diameter, and inversely proportional to the distance between the pressure spheres and the opening.
3. Stress concentrations can be relocated from the weak opening surface to stronger, confined wall rock using a dual ring pressurized sphere arrangement. In this arrangement, lower pressure inner spheres serve to block the radial component of the induced stress, thereby ensuring that the induced stress orientation is primarily tangential to the opening. This tangential loading causes rock to displace away from the area of the planned opening, reducing tangential stress concentrations on the opening surface once it is created.
4. Pressurization can be used to mitigate the unfavorable effects of a biaxial stress field. Placing pressure spheres in line with the minimum principal stress direction reduces the difference in magnitude between the minimum and maximum principal stresses and results in a more uniform stress distribution on the opening surface.
5. A single ring of pressurized spheres can be used to counteract the tangential tensile stresses induced by internally loaded openings.

The numerical modeling analysis performed was two-dimensional, and assumed linear elastic properties for the rock mass. More sophisticated modeling approaches could be used to study the pressurization process in more detail. However, it would be premature to perform such complex analyses before practical aspects of the pressurized sphere concept are more thoroughly investigated.

The laboratory portion of the investigation was designed to provide information on pressure sphere formation that would either validate or improve upon the assumptions used in the numerical modeling analysis. Fracturing experiments were performed on both confined and unconfined concrete cubes using sulfur as the fracturing fluid. Results of the laboratory investigation were largely inconclusive; the basic assumptions of the pressurized sphere concept were neither validated nor refuted. Nevertheless, the laboratory investigation produced the following information:

1. Molten sulfur can be used to induce hydraulic fracturing.
2. The viscosity spike associated with elevated temperatures can cause sulfur pumpability problems.

Although the laboratory program was unsuccessful in demonstrating pressure sphere creation, the problems encountered could likely be overcome with further research. Further research should also focus on alternatives to sulfur as a fracturing fluid. Hydraulic fracturing with sulfur was shown to be possible; however, the viscosity-related problems encountered suggest that other materials, such as wax, could be used with more success.

In conclusion, rock pressurization has good potential as a method for controlling the magnitude and location of stresses around underground excavations. This investigation provides justification for further research by demonstrating specific applications for rock pressurization, identifying its underlying mechanisms, and documenting the effects of sphere pressure, size, and location on the induced stress distribution. Until active stress control methods such as rock pressurization can be fully developed and applied in the field, improved excavation designs that fully exploit the advantages of confined rock strength will not be realized.

## ACKNOWLEDGMENTS

The author extends his sincere appreciation and gratitude to everyone who assisted in the completion of this work, especially Dr. John F. Abel, Jr., Professor Emeritis, Colorado School of Mines, and Martin S. Oudenhoven, mining engineer, Denver Research Center (retired), U.S. Bureau of Mines. They provided the inspiration, insight, and advice that made this publication possible.

# REFERENCES


1. Colgate, S. A. Method of Bulking or Caving a Volume of Subsurface Material. U.S. Pat. 3,616,855, Nov. 2, 1971.

2. Whiting, J. M. Method for Counterstressing In Situ Rock for Support of Underground Openings. U.S. Pat. 3,568,450, Mar. 9, 1971.

3. Reed, J. J. Mine-Opening Stabilization by Stress Redistribution. CO Sch. Mines Q., v. 51, No. 3, July 1956, pp. 63-97.

4. Obert, L. O., W. I. Duvall, and R. H. Merrill. Design of Underground Openings in Competent Rock. USBM B 587, 1960, 36 pp.

5. Holland, C. T. Cause and Occurrence of Coal Mine Bumps. Trans. AIME, v. 211, 1956, pp. 994-1004.

6. Obert, L. O., and W. I. Duvall. Rock Mechanics and the Design of Structures in Rock. Wiley, 1967, 650 pp.

7. Roux, A. J. A., and H. G. Denkhaus. An Investigation into the Problem of Rock Bursts, An Operational Research Project - Part II, An Analysis of the Problem of Rock Bursts in Deep Level Mining. J. Chem. Met. and Min. Soc., S. Afr., v. 55, No. 5, 1954.

8. Mauck, H. E. Coal Mine Bumps Can Be Eliminated. Trans. AIME, v. 211, 1958, pp. 993-994.

9. Serata, S. Stress Control Technique - An Alternative to Roof Bolting? Min. Eng. (Littleton, CO), v. 28, No. 5, May 1976, pp. 51-56.

10. Talman, W. G., and J. L. Schroder. Control of Mountain Bumps in the Pocahontas No. 4 Seam. Trans. AIME, v. 211, 1958, pp. 888-891.

11. Wang, F. D., D. M. Ropchan, and M. C. Sun. Proposed Technique for Improving Coal-Mine Roof Stability by Pillar Softening. Trans. AIME, v. 255, Mar. 1974, pp. 59-63.

12. Peperakis, J. Mountain Bumps at the Sunnyside Mines. Trans. AIME, v. 211, 1958, pp. 982-986.

13. Blake, W. Destressing Test at the Galena Mine, Wallace, Idaho. Trans. AIME, v. 252, 1972, pp. 294-299.

14. Morley, L. A., and J. E. Wilson. Control of Bumps. Ch. in SME Mining Engineering Handbook, ed. by A. B. Cummins and I. A. Givens. SME-AIME, N.Y., 1973, pp. 13-118 - 13-124.

15. Handin, J., and R. V. Hager, Jr. Experimental Deformation of Sedimentary Rocks Under Confining Pressure: Tests at Room Temperature on Dry Samples. Bull. Am. Assoc. Pet. Geol., v. 41, No. 1, Jan. 1957, pp. 1-50.

16. Oudenhoven, M. S., and T. L. Vandergrift. Rock Pressurization: A Method for Stress Control in Underground Structures. Paper in International Symposium on Unique Underground Structures (Denver, CO, June 12-15, 1990). CSM Press, Golden, CO, 1990, pp. 76-1 to 76-13.

17. Colgate, S. A. Method of Pressurizing and Stabilizing Rock by Periodic and Repeated Injections of a Settable Fluid of Finite Gel Strength. U.S. Pat. 4,370,077, Jan. 25, 1983.

18. Colgate, S. A., and N. K. Bowers. An Operational Test of Stress Field Engineering. Preprint, New Mexico Tech., Socorro, NM, 1976, 19 pp; available from T. L. Vandergrift, USBM Denver Research Center, Denver, CO.

19. Colgate, S. A., A. G. Petschek, R. V. Browning, and N. K. Bowers. Underground Stress Engineering: The Lifting and Stabilization of Underground Voids. Pres. at Conference on Energy and Mineral Resource Recovery, Golden, CO, Apr. 12-14, 1977. Los Alamos Scientific Laboratory preprint LA-UR-77-844, 12 pp.

20. Colgate, S. A. The Strengthening and Repair of Underground Structures: A New Approach to the Management of Nuclear Waste. Pres. at Sixth International Conference on Emerging Nuclear Energy Systems, Monterey, CA, June 16-21, 1991. Los Alamos National Laboratory preprint LA-UR-91-2755, 11 pp.

21. ___. In Situ Solution Mining of Coal. U.S. Pat. 3,973,628, Aug. 10, 1976.

22. Campbell, J. R., S. A. Colgate, and B. M. Wheat. Subterranean Stress Engineering Experiments. Paper in 13th Canadian Rock Mechanics Symposium (Toronto, Ontario, May 28-29, 1980). Harpell's Press Cooperative, Ste Anne de Bellevue, Quebec, 1980, pp. 31-35.

23. Hoek, E., and E. T. Brown. Underground Excavations in Rock. Inst. of Min. and Metall., London, 1980, 527 pp.

24. Thrasher, J. E., and R. B. Lange. Evaluation of Hard-Rock-Cavern Construction Methods for Compressed Air Energy Storage. EPRI Rep. No. AP-5717, Project 2488-11, Apr. 1988, 97 pp.

25. Karol, R. H. Chemical Grouting. Dekker, New York, 1990, 352 pp.

26. Tokoro, T., S. Kashima, and M. Murata. Grouting Method by Using the Flash-Setting Grout. Paper in Conference on Grouting in Geotechnical Engineering (New Orleans, LA, Feb. 10-12, 1982). ASCE, New York, NY, 1982, pp. 738-752.

27. Houlsby, A. C. Construction and Design of Cement Grouting. Wiley, 1990, 442 pp.

28. Morse, D. E. Sulfur. USBM Annu. Rep., 1991, 26 pp.

29. Freeport Sulphur Company. The Sulphur Data Book, comp. ed. by W. N. Tuller. McGraw-Hill, 1954, 143 pp.

30. Fanelli, R. Modifying the Viscosity of Sulfur. Ind. and Eng. Chemistry, v. 38, No. 1, Jan. 1946, pp. 39-43.

31. Gidley, J. L., S. A. Holditch, D. E. Nierode, and R. W. Veatch, Jr. Recent Advances in Hydraulic Fracturing. SPE Monograph Series, v. 12, 1989, 452 pp.

32. Haimson, B. C. Hydraulic Fracturing in Porous and Non-Porous Rock and Its Potential for Determining In Situ Stresses at Great Depth. Ph.D. Thesis, Univ. MN, Minneapolis, MN. U.S. Army Corps of Eng. Tech. Rep. 4-68, Missouri River Division, 1968, 233 pp.

33. MathSoft, Inc. (Cambridge, MA). MathCad User's Manual, Mechanical Engineering Applications Pack: Machine Design, Fluid Flow, and Heat Transfer. 1990, pp. 27-30.

34. Crouch, S. L., and A. M. Starfield. Boundary Element Methods in Solid Mechanics. Allen and Urwin, London, 1983, 322 pp.

35. Curran, J. H., and B. T. Corkum. EXAMINE - A 2D Boundary Element Program for Calculating Stresses around Underground Excavations in Rock. Data Visualization Laboratory, Univ. of Toronto, 1991, 72 pp.

36. Sneddon, I. N., and M. Lowengrub. Crack Problems in the Classical Theory of Elasticity. Wiley, 1969, 221 pp.

37. Shaffer, R. J., A. G. Petschek, and S. A. Colgate. Alteration of Underground Stresses by Hydrofracturing. Report to the New Mexico Energy Commission, Final Report of Grant "In Situ Solution Mining of Coal," NM Tech., Socorro, NM, Sept. 1975, pp. 10-38.

# APPENDIX A.—MODELING PROGRAM, ASSUMPTIONS, AND RESULTS

## PROGRAM DESCRIPTION

The fictitious stress boundary-element method was chosen for this work because of its suitability to underground stress analysis problems, its simple input structure, and the ease in which model parameters can be varied to perform parametric analyses. Mathematical details of the method are beyond the scope of this report; an excellent explanation is given by Crouch (*34*).[1]

The particular boundary-element program used in this study, EXAMINE$^{2D}$,[2] was developed at the University of Toronto as a parametric analysis tool for investigating stresses and displacements around excavations in rock (*35*).

EXAMINE performs a plane strain analysis, which means that the model is assumed to extend infinitely in the direction normal to the section of analysis. For example, in modeling Colgate's "pressure spheres" in two dimensions, the spheres are represented by pressurized holes of circular cross section. In a plane strain analysis, these models really represent "pressure cylinders" whose long axes run parallel to the long axis of the excavation. Modeling an object such as a sphere in a plane strain analysis introduces errors because stresses are only allowed to "flow" around the object in the plane of analysis. This results in an exaggeration of induced stress magnitudes. So long as this exaggeration is kept in mind, the analysis can provide useful information about stress distribution trends.

The analysis performed by EXAMINE assumes that the material being modeled is homogeneous, isotropic, and linear elastic. Of course, these assumptions do not strictly hold true for any rock mass. Nevertheless, the stresses calculated by EXAMINE can be used to compare one excavation scenario to another and to show the effects of input parameter variation on the induced stress distribution. It should also be noted that the displacements calculated by the program are due solely to elastic deformation. In the real world, elastic displacements may only account for a small fraction of the displacements observed. Therefore, the displacement vectors shown in this analysis are meant to illustrate relative trends rather than absolute magnitudes.

EXAMINE dictates that one of the principal stress directions must be aligned with the long axis of the excavation, which means that the other two principal stress directions lie in the analysis section. However, the inclination of the in-plane principal stresses can be user-defined.

Although the program does not allow inelastic behavior (yielding and failure) to be modeled, it identifies areas where such behavior is likely by calculating strength factors. Using the Mohr-Coulomb failure criterion, the strength factor is defined as the ratio of the maximum internal shear stress at failure for a given point to the maximum internal shear stress developed at that point. On a Mohr diagram (figure A-1), the induced state of stress is represented by the circle centered at

$$P = ( \sigma_1 + \sigma_3 )/2 , \qquad \text{(A-1)}$$

where $P$ = mean stress,

$\sigma_1$ = maximum (most compressive) principal stress,

and $\sigma_3$ = minimum (least compressive) principal stress.

The diameter of the circle is defined by $\sigma_1$ and $\sigma_3$, which lie on opposite radii of the circle. The maximum shear stress developed for this condition can be calculated as

$$S = ( \sigma_1 - \sigma_3 )/2 . \qquad \text{(A-2)}$$

The maximum shear stress at failure, $S_m$, is represented by the radius of the largest circle centered at P that can be drawn tangent to the Mohr-Coulomb failure envelope. The Mohr-Coulomb failure envelope is defined by the line

$$\tau = c + \sigma \tan \phi , \qquad \text{(A-4)}$$

where $\tau$ = shear stress,

$c$ = cohesion,

[1]Italicized numbers in parentheses refer to items in the list of references preceding this appendix.

[2]Reference to specific products does not imply endorsement by the U.S. Bureau of Mines.

$\sigma$ = normal stress,

and $\phi$ = angle of internal friction.

$S_m$ is calculated as

$$S_m = c \cos\phi + P \sin\phi = [\sigma_{1(max)} - \sigma_{3(min)}]/2. \quad (A\text{-}4)$$

Again, the strength factor is defined as

$$\text{Strength Factor} = S_m/S. \quad (A\text{-}5)$$

The cohesion and the angle of internal friction are rock properties input by the user. Values of $\sigma_3$ smaller than the user-defined rock tensile strength, $\sigma_t$, indicate tensile, rather than shear failure. The strength factor for this condition is set to -1.

## ANALYSIS ASSUMPTIONS AND LIMITATIONS

As noted in the text, the modeled excavations were assumed to be in granite at a depth of 10,000 ft. The following properties were assumed:

$\upsilon$ = Poisson's ratio = 0.25,

E = Young's modulus = 41,400 MPa (6.0 $\times 10^6$ psi),

$\sigma_c$ = uniaxial compressive strength = 138 MPa (20,000 psi),

$\sigma_t$ = tensile strength = 13.8 MPa (2,000 psi), and

$\phi$ = angle of internal friction = 45°.

*Figure A-1*

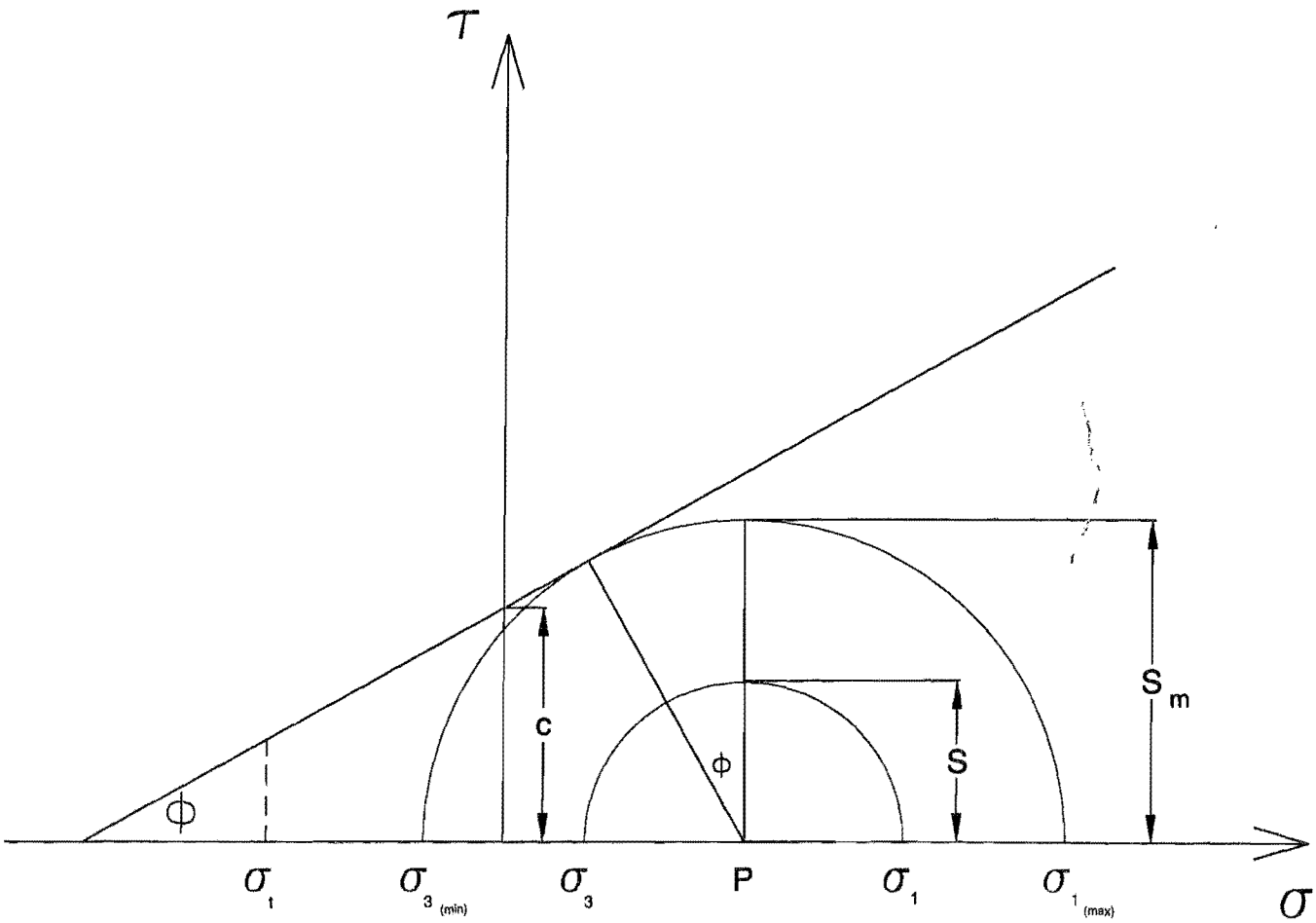


*Mohr-Coulomb failure criterion.*

Cohesion, c, is calculated in the program from the compressive strength and angle of internal friction as

$$c = \frac{\sigma_c}{2 \tan (45 + \phi/2)}. \qquad \text{(A-6)}$$

No attempt was made to estimate rock mass properties from these data; the rock mass as a whole would be much less competent due to natural fracturing. The difference between intact and in situ rock properties would not affect the calculation of stresses in this analysis since the stress distribution in an isotropic elastic medium is independent of the elastic constants E and $\upsilon$. Displacement calculations do depend on the elastic constants, however. Because of this and the fact that the program only accounts for elastic displacements, the displacements calculated are many times less than would be expected in the field. For these reasons, only relative displacements are presented and discussed.

Most of the cases modeled are symmetric about both the horizontal and vertical axes; due to this symmetry, only one-quarter of the problem must be represented. Contours are based on stress and displacement calculations at points in a rectangular grid in the modeled rock mass. Contours do not exhibit perfect symmetry because the geometry of the models is more suited to a grid based on polar coordinates.

## DEVELOPMENT OF THE PRESSURE SPHERE MODEL

To begin, it was assumed that the spheres could be modeled in two dimensions as four hydraulic fractures emanating from a central point and oriented 45° from one another (figure A-2). To estimate fracture widths and

*Figure A-2*

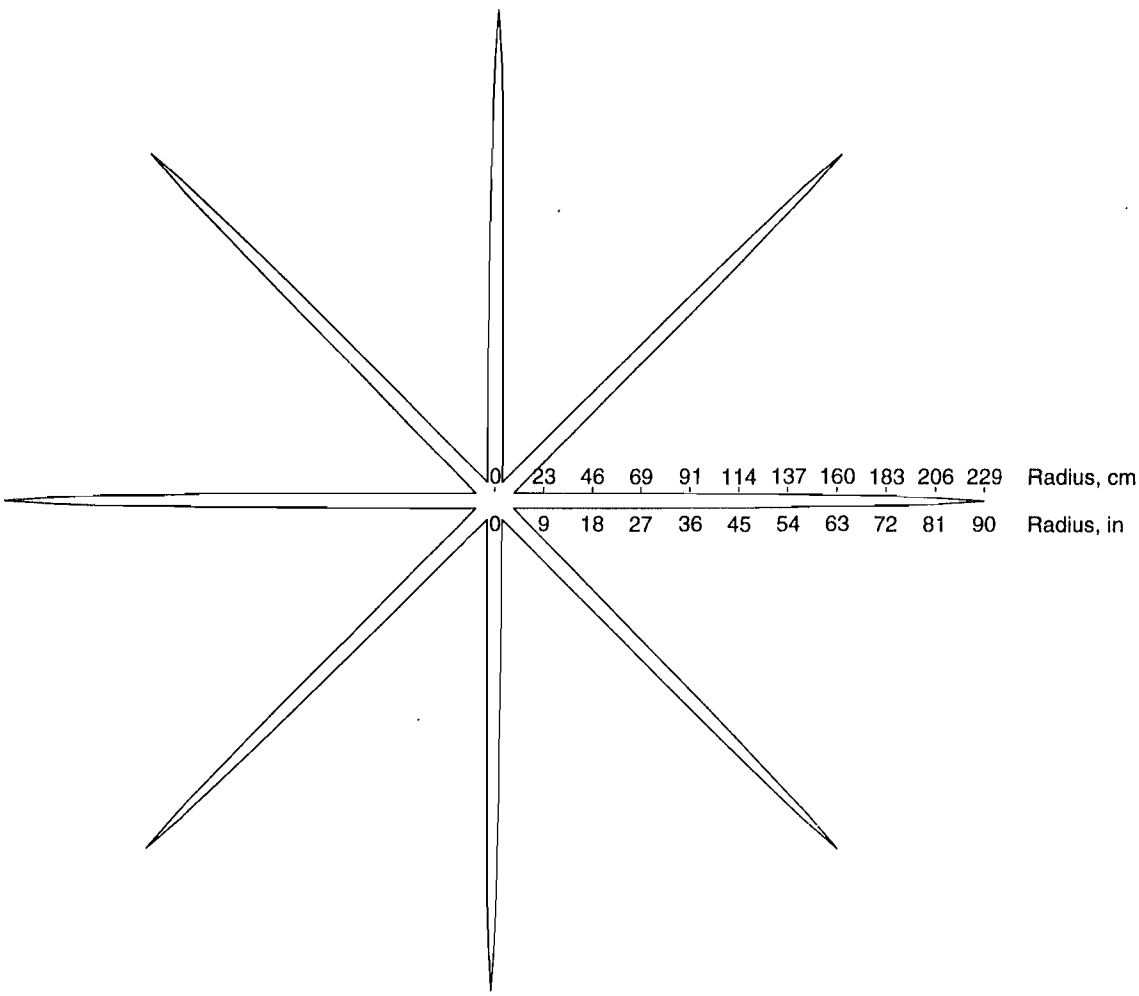


*Geometry of pressurized sphere model represented by four intersecting hydraulic fractures.*

internal pressures, a simple fracture propagation model, Sneddon's penny-shaped crack model (*36*), was used. A penny-shaped crack is defined as a flat disk-shaped fracture of elliptical cross section. Sneddon gives the width of a penny-shaped crack subject to constant internal pressure as

$$W = \frac{8C(P - \sigma)(1 - \nu^2)}{\pi E}\,[1 - (r/C)^2], \quad \text{(A-7)}$$

where $W$ = crack width at radius r, cm,

$C$ = fracture radius, cm,

$P$ = uniform internal crack pressure, MPa,

$\sigma$ = minimum effective stress, including pore pressure,

$\upsilon$ = Poisson's ratio,

$E$ = Young's modulus, MPa,

and $r$ = radius of interest, cm.

Although Sneddon's equation is based on a constant internal fracture pressure, in reality a pressure gradient exists along the length of the crack due to friction. Following a mathematical analysis presented by Shaffer (*37*), it was assumed that the pressure in the crack is proportional to the crack width.

Using the model input parameters mentioned before and an assumed fracture radius of 2.3 m (90 in), fracture widths and average pressures were calculated for each of 10 intervals along the fracture radius, as presented in table A-1.

Pressure in each interval was proportioned according to average fracture width in the interval, assuming an injection pressure of 620 MPa (90,000 psi). The maximum principal stress distribution for a single modeled fracture in a hydrostatic stress field of 6.9 MPa (10,000 psi) is shown in figure A-3. As expected, tensile stresses are induced near the crack ends and compressive stresses are induced normal to the fracture plane. It should be noted that in this and subsequent figures not all stress contours are shown. The EXAMINE postprocessor only allows six positive data contours to be displayed at once. When more detail is desired, another set of contours can be overlain. For example, the 480- and 550-MPa (70,000- and 80,000-psi) contours in the vicinity of the fracture are not shown in figure A-3.

**Table A-1.—Modeled fracture widths and pressures**

| r, cm (in) | W, cm (in) | Pressure in interval, MPa (psi) |
|---|---|---|
| 0 | 7.277 (2.865) | 619 (89,800) |
| 22.9 (9) | 7.239 (2.850) | 613 (88,900) |
| 45.7 (18) | 7.130 (2.807) | 600 (87,000) |
| 68.6 (27) | 6.942 (2.733) | 579 (84,000) |
| 91.4 (36) | 6.670 (2.626) | 552 (80,100) |
| 114.3 (45) | 6.302 (2.481) | 517 (74,900) |
| 137.2 (54) | 5.822 (2.292) | 469 (68,000) |
| 160.0 (63) | 5.197 (2.046) | 407 (59,000) |
| 182.3 (72) | 4.366 (1.719) | 321 (46,500) |
| 205.7 (81) | 3.172 (1.249) | 135 (19,600) |
| 228.6 (90) | 0 | |

r crack radius.
W crack width at radius r.

Figure A-4*A* shows the maximum principal stress distribution for a pressure sphere formed by four pressurized fractures. Radially oriented compressive stresses are induced in the rock mass outside the radius of the fractures. Tangential tensile stresses are also induced in this area (figure A-4*B*).

This pressure sphere model, based on gross but reasonable assumptions, supports the hypothesis that zones of above-normal, radially oriented compressive stresses can be induced by the formation of successive, reoriented, hydraulic fractures. However, creating this model in

EXAMINE was cumbersome because the coordinates of each segment end (196 in all) had to be calculated and input individually. In addition, the normal stress condition for each segment had to be input. To simplify the modeling process, an equivalent geometry was sought.

Figure A-5*A* shows the maximum principal stress distribution around a circular opening with a 2.3 m (90-in) radius and an internal hydrostatic pressure of 620 MPa (90,000 psi). The maximum principal stress distribution for the circular opening model is nearly identical to that of the fracture model. The same can be said of the minimum principal stress distribution (figure A-5*B*). Because of the equivalence of this simplified geometry, it was used to model the pressure spheres in all subsequent analyses.

***Figure A-3***

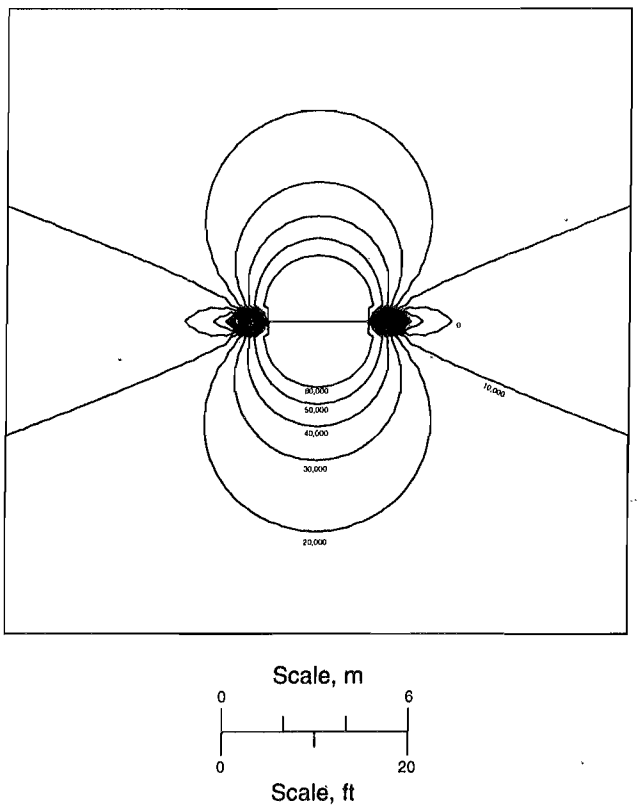


***Single pressurized crack in a 69-MPa (10,000-psi) hydrostatic stress field, maximum principal stress distribution.***

*Figure A-4*

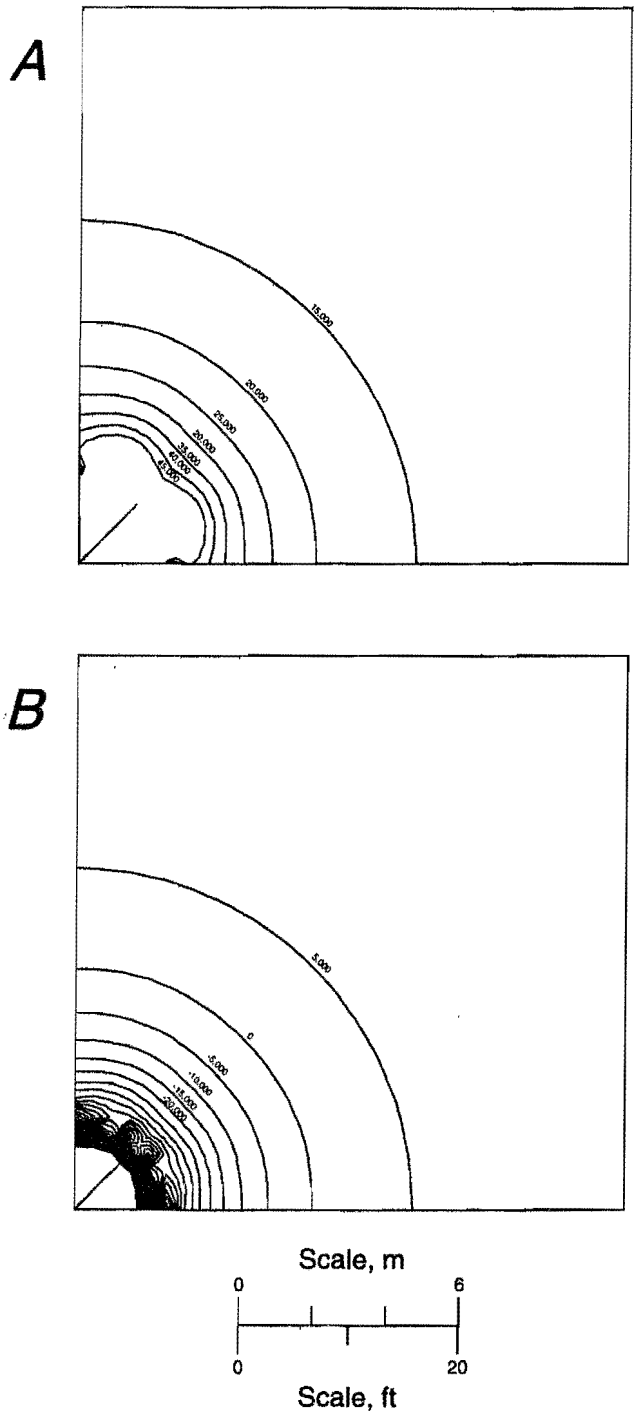


***Pressure sphere modeled as four intersecting pressurized cracks. A, Maximum principal stress distribution; B, minimum principal stress distribution.***

*Figure A-5*

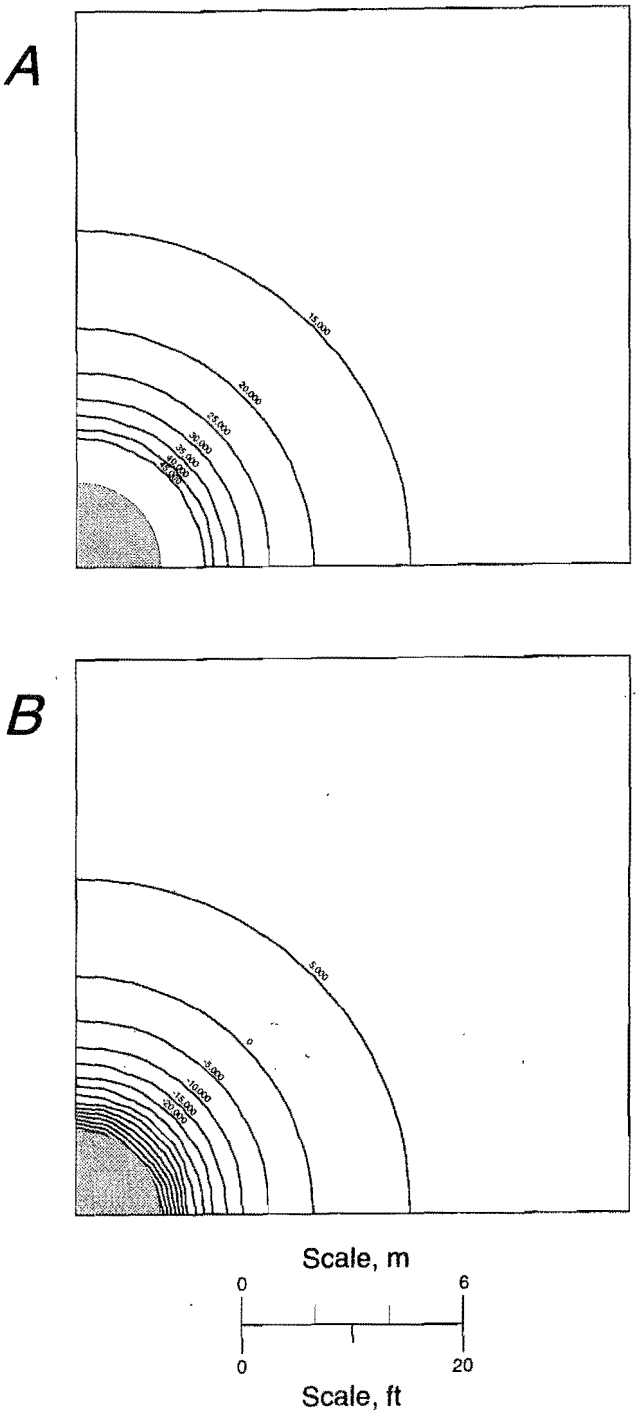


***Pressure sphere modeled as an internally loaded circular opening. A, Maximum principal stress distribution; B, minimum principal stress distribution.***

*Figure A-6*

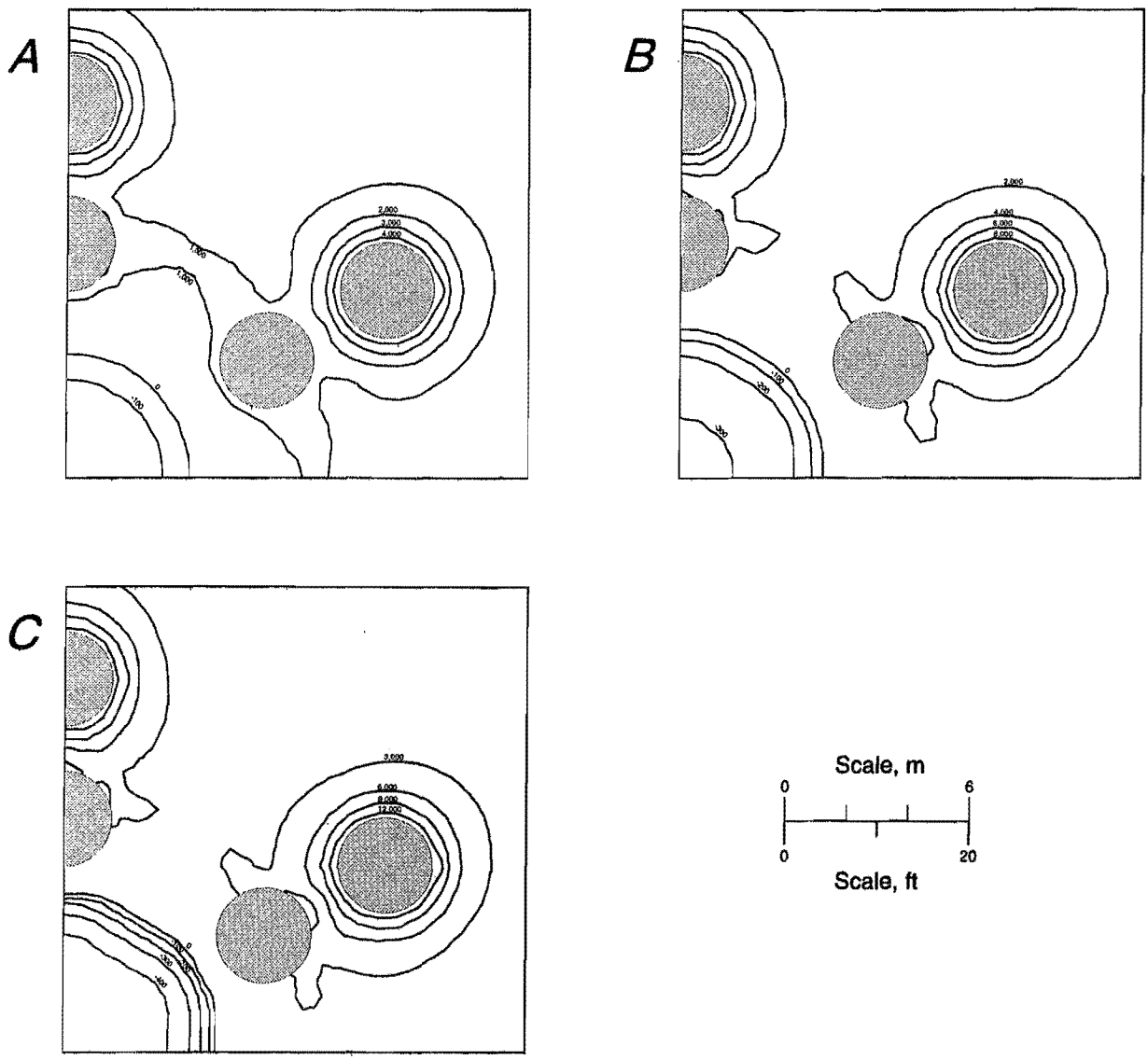


***Double ring of pressure spheres with inner sphere pressure of 10 MPa (1,500 psi) and outer sphere pressures of: A, 34 MPa (5,000 psi); B, 69 MPa (10,000 psi); and C, 103 MPa (15,000 psi); in a model with no opening or field stress, maximum principal stress distribution.***

*Figure A-7*

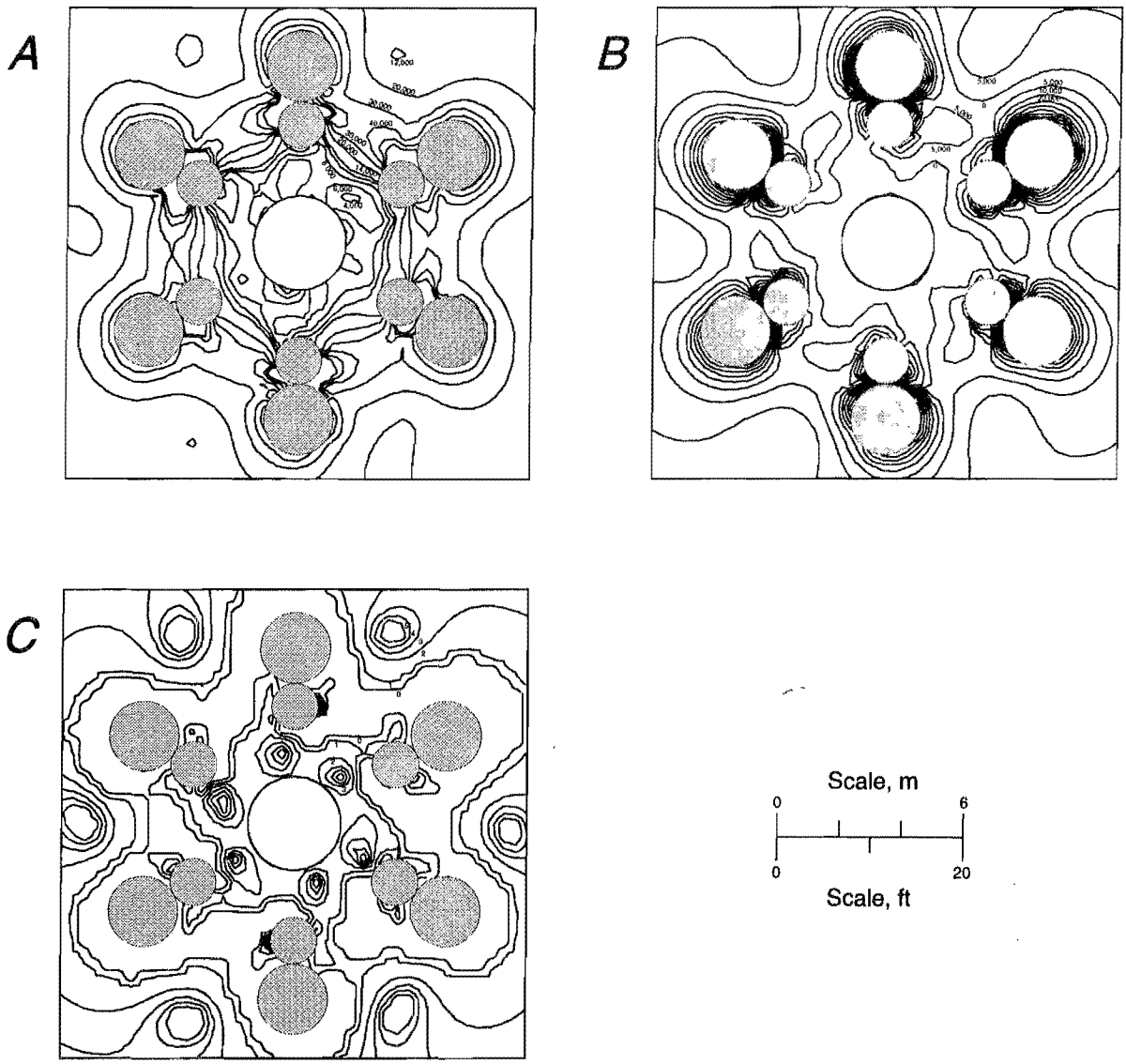


***Double ring of pressure spheres with nonuniform internal sphere loading surrounding a circular opening in a 69-MPa (10,000-psi) hydrostatic stress field. A, Maximum principal stress distribution; B, minimum principal stress distribution; C, strength factor distribution.***

*Figure A-8*

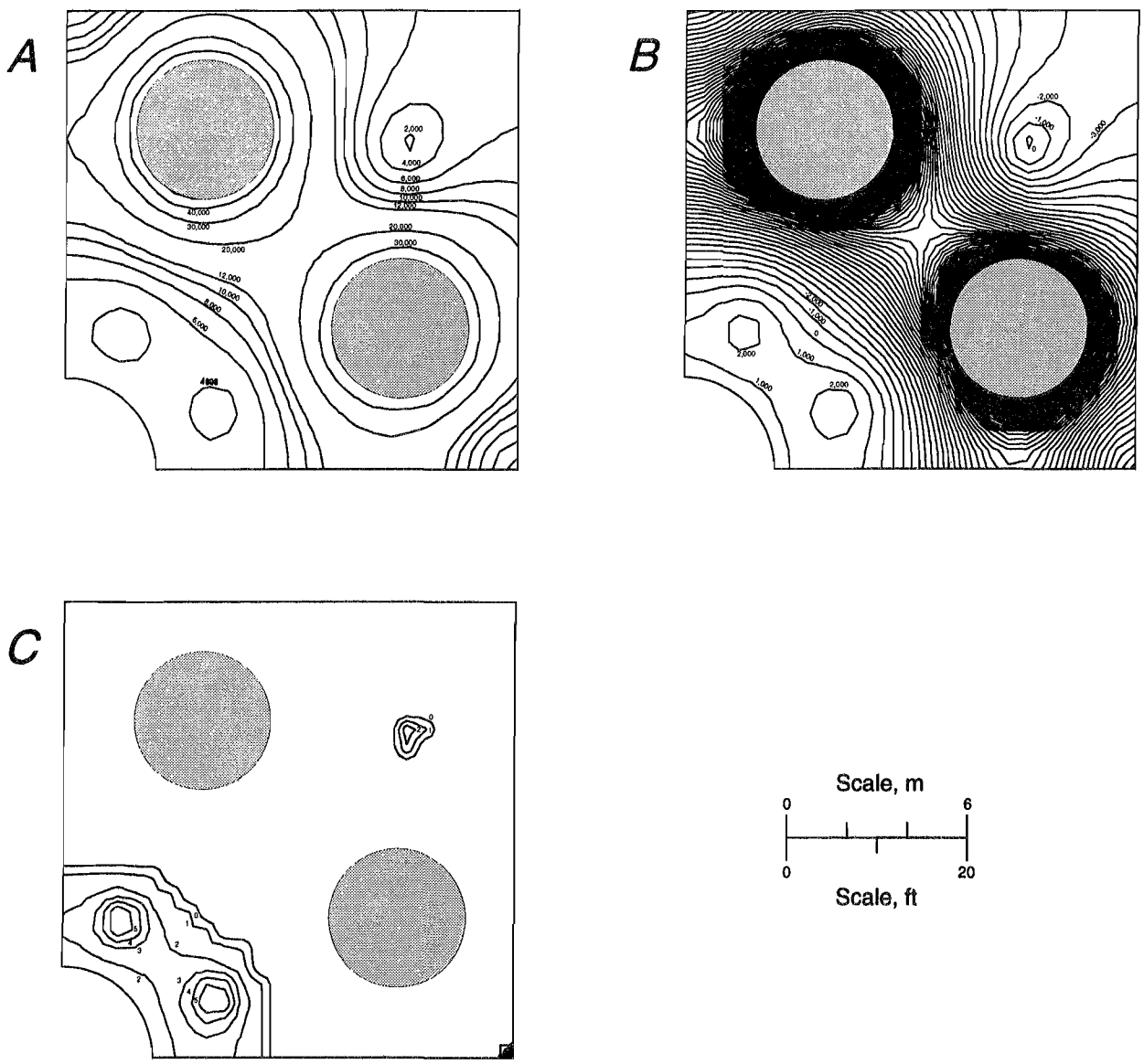


***Single ring of pressure spheres surrounding a circular opening internally loaded with 2.2-MPa (325-psi) air pressure. A, Maximum principal stress distribution; B, minimum principal stress distribution; C, strength factor distribution.***

# APPENDIX B.—FUNDAMENTALS OF HYDRAULIC FRACTURING

The process of repeated, reoriented hydraulic fracturing is based on relationships derived by analyzing the tangential stresses on the surface of a pressurized borehole. Haimson (*32*) gives the tangential stress on the surface of a pressurized cylindrical borehole in permeable rock as

$$\sigma_{\theta\theta} = 3\sigma_3 - \sigma_2 - \left[2 - \alpha \frac{1 - \nu}{1 - \nu}\right]\left[P_W\,(t) + P_0\right], \quad \text{(B-1)}$$

where $\sigma_{\theta\theta}$ = tangential stress (compression positive),

$\sigma_3$ = minimum principal stress in the plane perpendicular to the borehole axis,

$\sigma_2$ = maximum principal stress in the plane perpendicular to the borehole axis,

$\alpha$ = porosity constant,

$P_W$ = internal borehole pressure,

$P_0$ = pore pressure,

$\nu$ = Poisson's ratio,

and $t$ = time.

In laboratory experiments, Haimson found that hydraulic fracturing induced from a borehole packed off with a rubber packer is almost invariably along the axis of the borehole, even when the loading conditions would favor fracture perpendicular to the borehole. Away from the influence of the packer, fractures reorient so that they once again propagate perpendicular to the minimum principal stress direction. Because a rubber packer was used for the laboratory work performed in this study, it was assumed that the fractures induced would initially form along the axis of the borehole. Fracture formation and extension will occur in this direction when the tangential tensile stress at the surface of the borehole wall overcomes the tensile strength of the rock, $\sigma_t$. At the instant of fracture initiation ($t = t_c$), $\sigma_{\theta\theta} = -\sigma_t$ and the critical pressure $P_c = P_W(t_c)$. Therefore, the pressure criterion for fracturing along the borehole axis in permeable rock is

$$P_c = \frac{\sigma_t + 3\sigma_3 - \sigma_2}{2 - \alpha \dfrac{1 - 2\nu}{1 - \nu}} - P_0. \quad \text{(B-2)}$$

However, because of cooling and setting, rock is impermeable to molten sulfur. The criterion for fracture in impermeable rock is a special case of the criterion for permeable rock. In equation B-2 the term

$$2 - \alpha \frac{1 - 2\nu}{1 - \nu} \quad \text{(B-2)}$$

arises from the constitutive equations of continuum mechanics for fluid flow. In impermeable rock, there is no fluid flow into the rock, and the aforementioned term becomes unity. The critical pressure criterion for molten sulfur injection then becomes

$$P_c = \sigma_t + 3\sigma_3 - \sigma_2 - P_0. \quad \text{(B-3)}$$

In laboratory experiments, Haimson fractured blocks that contained a preexisting fracture plane. The value of the critical pressure and the direction of the hydraulic fracture were not affected so long as the borehole did not intersect the preexisting fracture plane. Several instances of hydraulic fracture propagation across the preexisting fracture plane were observed.